

Modeling a labyrinthine acoustic metamaterial through an inertia-augmented relaxed micromorphic approach

Mathematics and Mechanics of Solids
1–25

© The Author(s) 2023



Article reuse guidelines:

sagepub.com/journals-permissions

DOI: 10.1177/10812865221137286

journals.sagepub.com/home/mms**Jendrik Voss** *Institute for Structural Mechanics and Dynamics, Technical University Dortmund, Dortmund, Germany***Gianluca Rizzi** *Institute for Structural Mechanics and Dynamics, Technical University Dortmund, Dortmund, Germany***Patrizio Neff***Faculty of Mathematics, University of Duisburg-Essen, Essen, Germany***Angela Madeo***Institute for Structural Mechanics and Dynamics, Technical University Dortmund, Dortmund, Germany*

Received 13 September 2022; accepted 19 October 2022

Abstract

We present an inertia-augmented relaxed micromorphic model that enriches the relaxed micromorphic model previously introduced by the authors via a term $\text{Curl } \dot{P}$ in the kinetic energy density. This enriched model allows us to obtain a good overall fitting of the dispersion curves while introducing the new possibility of describing modes with negative group velocity that are known to trigger negative refraction effects. The inertia-augmented model also allows for more freedom on the values of the asymptotes corresponding to the cut-offs. In the previous version of the relaxed micromorphic model, the asymptote of one curve (pressure or shear) is always bounded by the cut-off of the following curve of the same type. This constraint does not hold anymore in the enhanced version of the model. While the obtained curves' fitting is of good quality overall, a perfect quantitative agreement must still be reached for very small wavelengths that are close to the size of the unit cell.

Keywords

Metamaterials, metastructure, inertia-augmented, relaxed micromorphic model, anisotropy, dispersion curves, band gap, parameters identification, generalized continua

1. Introduction

Metamaterials are materials whose mechanical properties go beyond those of classical materials thanks to their heterogeneous microstructure. They can show unusual static/dynamic responses such as negative Poisson's ratio

Corresponding author:

Jendrik Voss, Institute for Structural Mechanics and Dynamics, Technical University Dortmund, August-Schmidt-Str. 8, 44227 Dortmund, Germany.

Email: jendrik.voss@tu-dortmund.de

Table 1. Size, bulk material constants and wave speed for polyethylene unit cell where $\bar{\kappa}_B$ is the plane strain bulk modulus.^a

a	ρ	$\bar{\kappa}_B$	μ_B	$c_{p,B}$	$c_{s,B}$
(mm)	(kg/m ²)	(MPa)	(MPa)	(m/s)	(m/s)
20	900	3160	262	1950	540

^aThe relations between the wave speed and the elastic constants are $c_p = \sqrt{\frac{\bar{\kappa}_B + \mu_B}{\rho}} = \sqrt{\frac{\lambda_B + 2\mu_B}{\rho}}$ and $c_s = \sqrt{\frac{\mu_B}{\rho}}$, while the plane strain bulk modulus is $\bar{\kappa}_B = \lambda_B + \mu_B$.

[1], twist or bend in response to being pushed or pulled [2,3], band gaps [4–7], cloaking [8,9], focusing [10,11], channeling [12,13], negative refraction [14–16], etc. The working frequency of each metamaterial strongly depends on the characteristic size and the geometry of the underlying unit cell, as well as on the choice of the base material. In this paper, we present a labyrinthine metamaterial that, thanks to the use of a polymer-based material and an optimized distribution of mass inside the unit cell (see Figure 1), gives rise to a wide acoustic band gap with characteristic unit cell's size of the order of centimeters. Conceptually, similar geometries have already been explored in literature [17–22].

The direct finite element modeling of structures build up with this labyrinthine metamaterial is unfeasible due to the extremely tight meshing that would be needed to correctly cover the narrow strips of material inside each unit cell. It is thus apparent the need for a homogenized model to use this type of very promising metamaterials in actual engineering designs. Various homogenization techniques have been developed with the purpose of providing rigorous predictions of the macroscopic metamaterial's mechanical response when the properties of the base materials and their spatial distribution are known. These homogenization approaches have been shown to be useful in describing the overall behavior of metamaterials in the static and quasi-static regimes [23–35] as well as, more recently, in the dynamic regime [36–47]. However, these models are often unsuited to deal with finite-size metamaterials, because they are based on upscaling techniques valid for unbounded media. Because of that finite-size metamaterials' structures are mostly investigated via finite element simulations which are performed using directly the microstructured material [48]. The downside of this approach is that the computational cost quickly becomes unsustainable (especially for unit cells as the one presented in this paper), although the propagation patterns obtained are very accurate. This heavily limits the possibility of exploring large-scale or very convoluted geometric meta-structures.

To overcome this problem and open up the possibility of designing complex meta-structures using the metamaterial presented in this paper as a basic building block, we propose to use an inertia-augmented relaxed micromorphic model. This model is based on the relaxed micromorphic model that we previously established [49–53] and has been augmented with a new inertia term accounting for coupled space-time derivatives of the micro-distortion tensor. The relaxed micromorphic model has extensively proven its efficacy in describing the broadband behavior of many infinite and finitesize metamaterials [52–56] and is extended in this paper so as to be able to account for negative group velocity which was not the case before. We will show that the proposed model is able to describe well the labyrinthine metamaterial's response for a large range of frequencies (going beyond the first band gap) and wave numbers (approaching the size of the unit cell) and for all directions of propagation with a limited number of frequency- and scale-independent constitutive parameters. The new inertia-augmented term will be shown to trigger modes with negative group velocities that are known to be associated with negative refraction phenomena. The results presented in this paper will allow us to shortly present new designs of finite-size labyrinthine metamaterials' structures that can control elastic energy in the acoustic regime for eventual subsequent re-use.

1.1. A polyethylene-based metamaterial for acoustic control

In this section, we present a new unit cell's design that gives rise to a metamaterial for acoustic control. This unit cell is designed to achieve a band gap at relatively low frequencies (600 – 2000 Hz) so that application for acoustic control can be targeted. The unit cell considered is made out of polyethylene, cf. Table 1. Compared to aluminium or titanium, which we used for the metamaterials studied in literature [54–56], polyethylene gives rise to lower wave speeds, thus allowing band-gap phenomena to appear at lower frequencies.

A further lowering of the band gap is obtained through the adoption of a labyrinth-type geometry, cf. Figure 1. This structure presents a tetragonal symmetry and thus features a reduced number of parameters with respect to a fully anisotropic system. The circular center of the unit cell is connected by thin bars allowing the

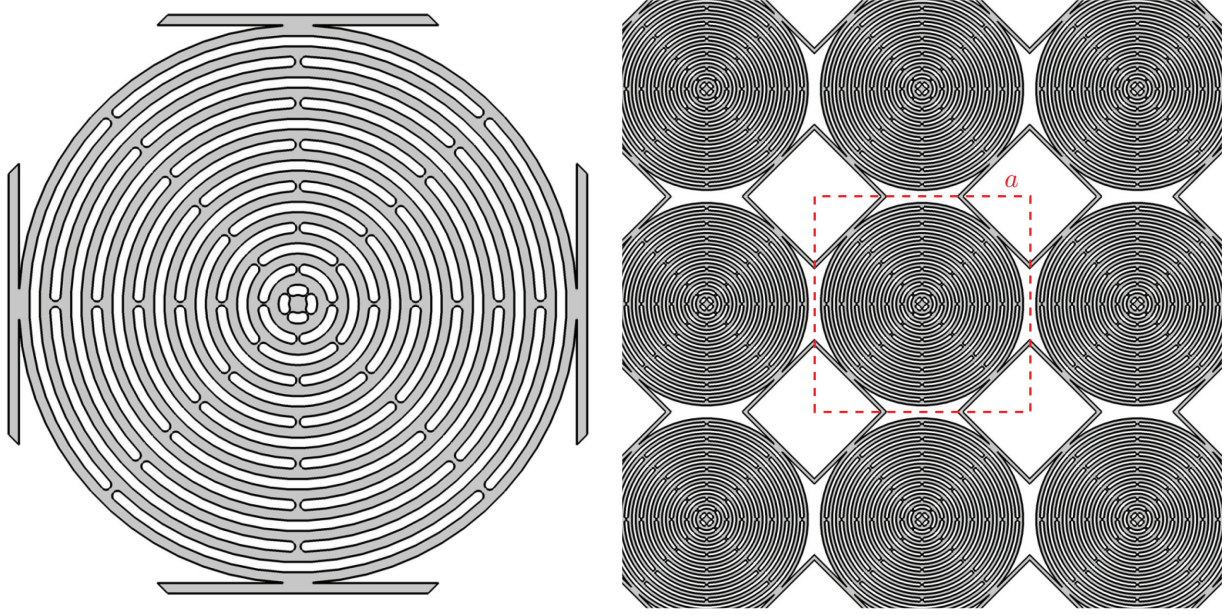


Figure 1. Geometry of the unit cell. Left: details of one unit cell (rotated by 45°) showing the tetragonal symmetry. For $a = 20\text{mm}$ as the size of the unit size we consider later, both the bars and holes have a thickness of 0.4mm each. Right: a 3×3 section of the metamaterial made up of this unit cell (red dashed square).

heavier center to move easily, thus giving rise to local resonance phenomena of relatively low frequencies while additionally providing a very soft macro-material behavior.

2. Relaxed micromorphic modeling of finite-size metamaterials

We briefly recall the weak and strong form of the governing equations of both classical Cauchy and relaxed micromorphic continua. The Lagrangian \mathcal{L}_c for the classical Cauchy model is

$$\mathcal{L}_c(\nabla u, \dot{u}) = \frac{1}{2}\rho \|\dot{u}\|^2 - \frac{1}{2}\langle \mathbb{C} \text{sym} \nabla u, \text{sym} \nabla u \rangle, \quad (1)$$

where u is the displacement field, $\langle \cdot, \cdot \rangle: \mathbb{R}^{n \times n} \times \mathbb{R}^{n \times n} \rightarrow \mathbb{R}$ is the scalar product, ρ is the apparent mass density, and \mathbb{C} is the classical fourth-order elasticity tensor. The Lagrangian \mathcal{L}_m for the relaxed micromorphic model enhanced with the micro-inertia term $\text{Curl } \dot{P}$ is [52–55]¹

$$\begin{aligned} \mathcal{L}_m(\dot{u}, \nabla \dot{u}, \dot{P}, \text{Curl } \dot{P}, \nabla u, P, \text{Curl } P) = & \frac{1}{2}\rho \|\dot{u}\|^2 + \frac{1}{2}\langle \mathbb{J}_m \text{sym } \dot{P}, \text{sym } \dot{P} \rangle + \langle \mathbb{J}_c \text{skew } \dot{P}, \text{skew } \dot{P} \rangle \\ & + \frac{1}{2}\langle \mathbb{T}_e \text{sym } \nabla \dot{u}, \text{sym } \nabla \dot{u} \rangle + \frac{1}{2}\langle \mathbb{T}_c \text{skew } \nabla \dot{u}, \text{skew } \nabla \dot{u} \rangle \\ & + \frac{1}{2}\langle \mathbb{M}_s \text{sym } \text{Curl } \dot{P}, \text{sym } \text{Curl } \dot{P} \rangle + \frac{1}{2}\langle \mathbb{M}_a \text{skew } \text{Curl } \dot{P}, \text{skew } \text{Curl } \dot{P} \rangle \\ & - \frac{1}{2}\langle \mathbb{C}_e \text{sym}(\nabla u - P), \text{sym}(\nabla u - P) \rangle \\ & - \frac{1}{2}\langle \mathbb{C}_c \text{skew}(\nabla u - P), \text{skew}(\nabla u - P) \rangle - \frac{1}{2}\langle \mathbb{C}_{\text{micro}} \text{sym } P, \text{sym } P \rangle \\ & - \frac{1}{2}\langle \mathbb{L}_s \text{sym } \text{Curl } P, \text{sym } \text{Curl } P \rangle - \frac{1}{2}\langle \mathbb{L}_a \text{skew } \text{Curl } P, \text{skew } \text{Curl } P \rangle, \end{aligned} \quad (2)$$

where $u \in \mathbb{R}^3$ is the macroscopic displacement field; $P \in \mathbb{R}^{3 \times 3}$ is the non-symmetric micro-distortion tensor; ρ is the macroscopic apparent density; $\mathbb{J}_m, \mathbb{J}_c, \mathbb{T}_e, \mathbb{T}_c, \mathbb{M}_s, \mathbb{M}_a$ are fourth-order micro-inertia tensors; and $\mathbb{C}_e, \mathbb{C}_c,$

$\mathbb{C}_{\text{micro}}$, \mathbb{L}_s , and \mathbb{L}_a are fourth-order elastic tensors (for more details see Appendix 1).² The action functional \mathcal{A}_i of the considered continuum can be defined based on the Lagrangian function \mathcal{L}_i and the external work \mathcal{U}_i as

$$\mathcal{A}_c = \int_{\Omega \times [0, T]} \mathcal{L}_c \, dx \, dt - \int_0^T \mathcal{U}_c^{\text{ext}} \, dt, \quad \text{and} \quad \mathcal{A}_m = \int_{\Omega \times [0, T]} \mathcal{L}_m \, dx \, dt - \int_0^T \mathcal{U}_m^{\text{ext}} \, dt, \quad (3)$$

for classical Cauchy and relaxed micromorphic media, respectively. In equation (3), $\Omega \subset \mathbb{R}^3$ is the domain of the considered continuum in its reference configuration and $[0, T]$ is a time interval during which the deformation of the continuum is observed. In the case of a conservative system, the virtual work of internal actions $\mathcal{W}_i^{\text{int}} = \delta \mathcal{L}_i$ can be defined as the first variation of the Lagrangian function, while the virtual work of external actions $\mathcal{W}_i^{\text{ext}} = \delta \mathcal{U}_i^{\text{ext}}$ is given as the first variation of the external work. In formulas, we have

$$\delta \mathcal{A}_c = \int_0^T \mathcal{W}_c^{\text{int}} \, dt - \int_0^T \mathcal{W}_c^{\text{ext}} \, dt, \quad \text{and} \quad \delta \mathcal{A}_m = \int_0^T \mathcal{W}_m^{\text{int}} \, dt - \int_0^T \mathcal{W}_m^{\text{ext}} \, dt, \quad (4)$$

for classical Cauchy and relaxed micromorphic media, respectively. In equation (4), the variation operator δ indicates that the variation must be taken with respect to the unknown kinematics fields (u for Cauchy media and (u, P) for the relaxed micromorphic model). Following classical variational calculus, the strong form of the bulk equations of motion and the Neumann boundary conditions for the Cauchy and the relaxed micromorphic model can be obtained via a least action principle stating that the first variation of the action functional must be vanishing. In absence of external body loads, the application of a least-action principle to Cauchy and relaxed micromorphic models gives the following equilibrium equation: [49, 53, 54]

$$\rho \ddot{u} = \text{Div } \sigma, \quad \sigma := \mathbb{C} \, \text{sym } \nabla u, \quad (5)$$

for the classical Cauchy model, and

$$\rho \ddot{u} - \text{Div } \hat{\sigma} = \text{Div } \tilde{\sigma}, \quad \bar{\sigma} = \tilde{\sigma} - s - \text{Curl } m - \text{Curl } \hat{m}, \quad (6)$$

for the relaxed micromorphic model, where we set

$$\begin{aligned} \tilde{\sigma} &:= \mathbb{C}_c \, \text{sym}(\nabla u - P) + \mathbb{C}_c \, \text{skew}(\nabla u - P), & \hat{\sigma} &:= \mathbb{T}_e \, \text{sym } \nabla \ddot{u} + \mathbb{T}_c \, \text{skew } \nabla \ddot{u}, \\ \bar{\sigma} &:= \mathbb{J}_m \, \text{sym } \ddot{P} + \mathbb{J}_c \, \text{skew } \ddot{P}, & s &:= \mathbb{C}_{\text{micro}} \, \text{sym } P, \\ m &:= \mathbb{L}_s \, \text{sym } \text{Curl } P + \mathbb{L}_a \, \text{skew } \text{Curl } P, & \hat{m} &:= \mathbb{M}_s \, \text{sym } \text{Curl } \ddot{P} + \mathbb{M}_a \, \text{skew } \text{Curl } \ddot{P}. \end{aligned} \quad (7)$$

The Neumann boundary condition for the classical Cauchy model are

$$t_c := \sigma n = t_c^{\text{ext}}, \quad (8)$$

with t_c^{ext} as the externally applied traction vector and n as the outward-pointing normal to the boundary, and for the relaxed micromorphic model

$$t_m := (\tilde{\sigma} + \hat{\sigma}) n = t_m^{\text{ext}} \quad \text{and} \quad \tau := (m + \hat{m}) \times n = \tau^{\text{ext}}, \quad (9)$$

where t_m^{ext} is the generalized traction vector, τ^{ext} is the double traction second-order tensor, and the cross product \times is understood row-wise. In absence of curvature terms ($\mathbb{L}_s = \mathbb{L}_a = \mathbb{M}_s = \mathbb{M}_a = 0$), the boundary condition (9)₂ involving τ must not be assigned on the boundary.

As it is well known, Dirichlet-type boundary conditions can also be alternatively considered in the form $u = u^{\text{ext}}$ for Cauchy media, while $u = u^{\text{ext}}$ and $P \times n = \phi^{\text{ext}}$ for the relaxed micromorphic model where n is the outward-pointing normal vector to the surface and ϕ^{ext} is an assigned second-order tensor.

2.1. Tetragonal symmetry / shape of elastic tensors (in Voigt notation)

In the following equation (10), we report the elastic tensors expressed in Voigt notation for the tetragonal class of symmetry³, where only the parameters involved under the plane strain hypothesis are explicitly presented. Thereby, the symbol \star indicates that the specific entry do not intervene under the plane strain hypothesis.⁴ The class of symmetry has been chosen accordingly with the symmetry of the unit cell presented in Figure 1, under the assumption that the same class of symmetry applies both at the micro- and the macro-scale.

$$\begin{aligned}
\mathbb{C}_e &= \begin{pmatrix} \kappa_e + \mu_e & \kappa_e - \mu_e & \star & \dots & 0 \\ \kappa_e - \mu_e & \kappa_e + \mu_e & \star & \dots & 0 \\ \star & \star & \star & \dots & 0 \\ \vdots & \vdots & \vdots & \ddots & \vdots \\ 0 & 0 & 0 & & \mu_e^* \end{pmatrix}, & \mathbb{C}_{\text{micro}} &= \begin{pmatrix} \kappa_m + \mu_m & \kappa_m - \mu_m & \star & \dots & 0 \\ \kappa_m - \mu_m & \kappa_m + \mu_m & \star & \dots & 0 \\ \star & \star & \star & \dots & 0 \\ \vdots & \vdots & \vdots & \ddots & \vdots \\ 0 & 0 & 0 & & \mu_m^* \end{pmatrix}, \\
\mathbb{J}_m &= \rho L_c^2 \begin{pmatrix} \kappa_\gamma + \gamma_1 & \kappa_\gamma - \gamma_1 & \star & \dots & 0 \\ \kappa_\gamma - \gamma_1 & \kappa_\gamma + \gamma_1 & \star & \dots & 0 \\ \star & \star & \star & \dots & 0 \\ \vdots & \vdots & \vdots & \ddots & \vdots \\ 0 & 0 & 0 & & \gamma_1^* \end{pmatrix}, & \mathbb{T}_e &= \rho L_c^2 \begin{pmatrix} \bar{\kappa}_\gamma + \bar{\gamma}_1 & \bar{\kappa}_\gamma - \bar{\gamma}_1 & \star & \dots & 0 \\ \bar{\kappa}_\gamma - \bar{\gamma}_1 & \bar{\kappa}_\gamma + \bar{\gamma}_1 & \star & \dots & 0 \\ \star & \star & \star & \dots & 0 \\ \vdots & \vdots & \vdots & \ddots & \vdots \\ 0 & 0 & 0 & & \bar{\gamma}_1^* \end{pmatrix}, \\
\mathbb{L}_s &= L_c^2 \begin{pmatrix} \star & \star & \star & \dots & 0 \\ \star & \star & \star & \dots & 0 \\ \star & \star & \star & \dots & 0 \\ \vdots & \vdots & \vdots & \alpha_1 & 0 \\ 0 & 0 & 0 & 0 & \alpha_1 \\ 0 & 0 & 0 & 0 & 0 \\ & & & & \star \end{pmatrix}, & \mathbb{M}_s &= \rho L_c^4 \begin{pmatrix} \star & \star & \star & \dots & 0 \\ \star & \star & \star & \dots & 0 \\ \star & \star & \star & \dots & 0 \\ \vdots & \vdots & \vdots & \beta_1 & 0 \\ 0 & 0 & 0 & 0 & \beta_1 \\ 0 & 0 & 0 & 0 & 0 \\ & & & & \star \end{pmatrix}, & (10) \\
\mathbb{C}_c &= \begin{pmatrix} \star & 0 & 0 \\ 0 & \star & 0 \\ 0 & 0 & 4\mu_c \end{pmatrix}, & \mathbb{J}_c &= \rho L_c^2 \begin{pmatrix} \star & 0 & 0 \\ 0 & \star & 0 \\ 0 & 0 & 4\gamma_2 \end{pmatrix}, & \mathbb{T}_c &= \rho L_c^2 \begin{pmatrix} \star & 0 & 0 \\ 0 & \star & 0 \\ 0 & 0 & 4\bar{\gamma}_2 \end{pmatrix}, \\
\mathbb{L}_a &= L_c^2 \begin{pmatrix} 4\alpha_2 & 0 & 0 \\ 0 & 4\alpha_2 & 0 \\ 0 & 0 & \star \end{pmatrix}, & \mathbb{M}_a &= \rho L_c^4 \begin{pmatrix} 4\beta_2 & 0 & 0 \\ 0 & 4\beta_2 & 0 \\ 0 & 0 & \star \end{pmatrix}.
\end{aligned}$$

It is emphasized that the matrix representation of \mathbb{L}_s , \mathbb{L}_a , \mathbb{M}_s , and \mathbb{M}_a differs from the others since the non-zero terms in $(\text{Curl } P)_{ij}$ and in $(\text{Curl } \dot{P})_{ij}$ are the “out-of-plane curvatures” related to the indexes $i = 1, 2$ and $j = 3$. To better explain this fact, we consider the shape of $\text{Curl } m$ given by

$$\begin{aligned}
P &= \begin{pmatrix} \bullet & \bullet & 0 \\ \bullet & \bullet & 0 \\ 0 & 0 & 0 \end{pmatrix}, & \text{Curl } P &= \begin{pmatrix} 0 & 0 & \bullet \\ 0 & 0 & \bullet \\ 0 & 0 & 0 \end{pmatrix}, & (11) \\
m &= (\mathbb{L}_s + \mathbb{L}_a) \text{Curl } P = \begin{pmatrix} 0 & 0 & \bullet \\ 0 & 0 & \bullet \\ \bullet & \bullet & 0 \end{pmatrix}, & \text{Curl } m &= \begin{pmatrix} \bullet & \bullet & 0 \\ \bullet & \bullet & 0 \\ 0 & 0 & \bullet \end{pmatrix}.
\end{aligned}$$

Note that the structure of $\text{Curl } \hat{m} = \text{Curl}((\mathbb{M}_s + \mathbb{M}_a) \text{Curl } \dot{P})$ is identical.

As it can be seen from equation (11)₄, even if the sym/skew decomposition is enforced in the constitutive law (we recall that \mathbb{L}_s , \mathbb{L}_a , \mathbb{M}_s , and \mathbb{M}_a have minor symmetries, see Appendix 1), it is not guaranteed that the term $\text{Curl } m$ appearing in the equilibrium equations (6) will retain only in-plane components for the most general constitutive tensor belonging to the tetragonal symmetry class. In order to avoid this out-of-plane contribution, we must impose one of the following conditions:

$$\alpha_2 = \alpha_1 \quad \wedge \quad \beta_2 = \beta_1 \quad \text{or} \quad P_{22} = 0. \quad (12)$$

Since the condition (12)₂ is not desirable because it prevents the presence of pressure waves, the condition (12)₁ will be adopted. This choice, while reducing the number of parameters in the model, does not reduce the number of the independent ones for $\text{Curl } P$ and $\text{Curl } \dot{P}$ as shown in Appendix 1.

Furthermore, we can always compute the parameters⁵ of the meso-scale depending on the micro-parameters and a new set of macro-parameters [51,54,57]:

$$\mathbb{C}_e = \mathbb{C}_{\text{micro}} (\mathbb{C}_{\text{micro}} - \mathbb{C}_{\text{macro}})^{-1} \mathbb{C}_{\text{macro}}, \quad (13)$$

where $\mathbb{C}_{\text{macro}}$ has the same structure of $\mathbb{C}_{\text{micro}}$ and \mathbb{C}_e . For the tetragonal class of symmetry in 2D, relation (13) particularizes to

$$\mu_e = \frac{\mu_m \mu_M}{\mu_m - \mu_M}, \quad \kappa_e = \frac{\kappa_m \kappa_M}{\kappa_m - \kappa_M}, \quad \mu_e^* = \frac{\mu_m^* \mu_M^*}{\mu_m^* - \mu_M^*}, \quad (14)$$

In the limit of infinitesimal small unit cells or rather of an indefinitely large body, these macro-parameters are obtained as the homogenization to a classical Cauchy material [51,57] and can directly be obtained by the slope of the acoustic curves at the origin, cf. section 5.2. Throughout this paper, all material parameters introduced will be positive to guarantee the positive definiteness of their corresponding tensors.

3. Dispersion curves

We assume a plane strain⁶ time-harmonic ansatz for the displacement u and the micro-distortion tensor P

$$v_j = \Psi_j e^{i(k_1 x_1 + k_2 x_2 - \omega t)}, \quad (15)$$

where v_j represents the generic component of u or P , Ψ_j is a scalar amplitude, $(k_1, k_2)^T = k (\sin \phi, \cos \phi)^T$ are the wave vector components with ϕ as the angle giving the direction of propagation, k the wave vector length, and ω is the frequency.

Substituting the ansatz (15) in the equilibrium equations (6), we obtain the homogeneous algebraic linear system

$$A \Psi = 0 \quad (16)$$

where $A = A(\omega, k, \phi) \in \mathbb{C}^{6 \times 6}$ is the acoustic tensor which depends on the frequency ω , the wave vector length k , the angle of propagation ϕ , all the constitutive parameters in equation (10), and $\Psi \in \mathbb{R}^6$ is the vector of amplitudes.⁷ The non-trivial solutions of the system (16) are obtained when A is singular, i.e. when $\det A = 0$, which provides relations between $k = k(\omega, \phi)$ (or $\omega = \omega(k, \phi)$), the so-called dispersion relations.

The acoustic tensor can be written as follows:

$$A = \begin{pmatrix} B_1 & C_1 \\ C_2 & B_2 \end{pmatrix}, \quad (17)$$

where $(B_1, B_2, C_1, C_2) \in \mathbb{C}^{3 \times 3}$.

Since $\det A = \det(B_1) \det(B_2 - C_2 B_1^{-1} C_1)$ [58], it is clear that the determinant of A becomes the product of the two independent factors $\det B_1$ and $\det B_2$ if either $C_1 = 0$ or $C_2 = 0$. If the reference system is chosen to be aligned with the direction of the wave vector (i.e. $\phi = \theta$, with θ the angle of rotation of the reference system), the sub-matrices C_1 and C_2 expressions are as follows:

$$C_1 = \frac{\sin(4\theta)}{2} \begin{pmatrix} k^2 (q_e - L_c^2 \rho \bar{q}_\gamma \omega^2) & ikq_e & ikq_e \\ -ikq_e & -\rho L_c^2 q_\gamma \omega^2 + q_e + q_m & -\rho L_c^2 q_\gamma \omega^2 + q_e + q_m \\ ikq_e & \rho L_c^2 q_\gamma \omega^2 - q_e - q_m & \rho L_c^2 q_\gamma \omega^2 - q_e - q_m \end{pmatrix}, \quad (18)$$

$$C_2 = \frac{\sin(4\theta)}{2} \begin{pmatrix} k^2 (q_e - L_c^2 \rho \bar{q}_\gamma \omega^2) & ikq_e & -ikq_e \\ -ikq_e & -\rho L_c^2 q_\gamma \omega^2 + q_e + q_m & \rho L_c^2 q_\gamma \omega^2 - q_e - q_m \\ -ikq_e & -\rho L_c^2 q_\gamma \omega^2 + q_e + q_m & \rho L_c^2 q_\gamma \omega^2 - q_e - q_m \end{pmatrix},$$

where $q_e = \mu_e - \mu_e^*$, $q_m = \mu_m - \mu_m^*$, $q_\gamma = \gamma_1 - \gamma_1^*$, and $\bar{q}_\gamma = \bar{\gamma}_1 - \bar{\gamma}_1^*$. It is highlighted that, since the constitutive law for the curvature terms $\text{Curl}P$ and $\text{Curl}\dot{P}$ depends on just one parameter, they are isotropic, and this makes the matrices C_1 and C_2 independent with respect α_i and β_i , while the expressions of the latter in B_1 and B_2 are not affected by the rotation of the reference system.

From equation (18) it is possible to deduce that the condition for which $C_1 = C_2 = 0$ (one of the two would be already enough) is $\theta = (\pi n)/4$ with $n \in \mathbb{N}$. This means that, when the reference system is aligned with

the direction of wave propagation, and both are aligned with a symmetry axes of the material, the determinant $\det A = \det(B_1) \det(B_2)$ is the product of two independent factors.

These two independent factors can be associated with pure-pressure waves $\det(B_1)$ and pure-shear waves $\det(B_2)$.

In particular, this allows us to reduce the order of the dispersion polynomial by

$$\det A = p(k^2, k^4, k^6, k^8, \omega^2, \omega^4, \omega^6, \omega^8, \omega^{10}, \omega^{12}) = p_1(k^2, k^4, \omega^2, \omega^4, \omega^6) p_2(k^2, k^4, \omega^2, \omega^4, \omega^6), \quad (19)$$

where p_1 and p_2 are of the form

$$p_i = c_0 k^2 + c_1 k^4 - (c_2 + c_3 k^2 + c_4 k^4) \omega^2 + (c_5 + c_6 k^2 + c_7 k^4) \omega^4 - (c_8 + c_9 k^2 + c_{10} k^4) \omega^6, \quad (20)$$

easing the calculation of the roots of these polynomials significantly, i.e. the expressions of the dispersion curves. It is noted that we can always consider $k(\omega)$, instead of $\omega(k)$, for shorter analytical expression as we must only solve a quadratic equation (in k^2) and not a third-order polynomial (in ω^2) but use $\omega(k)$ for easier plotting and its natural split in three distinct expressions for each dispersion curve.

4. New considerations on the relaxed micromorphic parameters

In this section, we draw some useful considerations about the consistency of the relaxed micromorphic model with respect to a change of unit cell's size and of the material properties of the base material. The model's consistency is checked against a standard Bloch–Floquet analysis of the wave propagation performed using the unit cell described in section 1.1 with built in periodic Bloch–Floquet boundary conditions from *Comsol Multiphysics*[®].

The following two connections between the properties of the unit cell and the behavior of the dispersion curves can be drawn:

- The dispersion curves scale proportionally in ω with respect to the speed of the wave of the bulk material composing the unit cell;
- The dispersion curves scale inversely in both ω and k with respect to the size of the unit cell.

Both results are useful to avoid repeating the time-consuming fitting procedure when changing the size of the cell and the base material's properties while keeping the unit cell's geometry unchanged.

4.1. Consistency of the relaxed micromorphic model with respect to a change in the unit cell's bulk material properties

The dispersive properties of a microstructured isotropic Cauchy material depend exclusively and linearly on the wave speeds of the bulk material once its geometry is fixed. Indeed, as it is well known, the dispersion relatives can be always written as $\omega = k c_i$, $i = \{p, s\}$, where c_p and c_s are the pressure and shear wave speeds, respectively, defined as follows:

$$c_p := \sqrt{\frac{\kappa_M + \mu_M}{\rho}}, \quad c_s := \sqrt{\frac{\mu_M}{\rho}}, \quad k = \frac{\omega}{c_i}, \quad i = \{p, s\}. \quad (21)$$

This implies that by scaling the elastic coefficients by a constant a and the density by another constant b , we have

$$\tilde{c}_p := c_p \sqrt{\frac{a}{b}}, \quad \tilde{c}_s := c_s \sqrt{\frac{a}{b}}, \quad k = \sqrt{\frac{b}{a}} \frac{\omega}{c_i}, \quad i = \{p, s\}. \quad (22)$$

Therefore, the response of an effective model should also change accordingly. Thus, we observe that by multiplying all the relaxed micromorphic elastic coefficients ($\mathbb{C}_e, \mathbb{C}_c, \mathbb{C}_{\text{micro}}, \mathbb{L}_s, \mathbb{L}_a$) by a constant a and the apparent density ρ by another constant b , we can rewrite equation (20) as⁸

$$a^3(c_0 k^2 + c_1 k^4) - a^2 b(c_2 + c_3 k^2 + c_4 k^4) \omega^2 + a b^2(c_5 + c_6 k^2 + c_7 k^4) \omega^4 - b^3(c_8 + c_9 k^2 + c_{10} k^4) \omega^6 = 0. \quad (23)$$

By collecting a^3 we obtain

$$a^3 \left[(c_0 k^2 + c_1 k^4) - (c_2 + c_3 k^2 + c_4 k^4) \left(\omega \sqrt{\frac{b}{a}} \right)^2 + (c_5 + c_6 k^2 + c_7 k^4) \left(\omega \sqrt{\frac{b}{a}} \right)^4 - (c_8 + c_9 k^2 + c_{10} k^4) \left(\omega \sqrt{\frac{b}{a}} \right)^6 \right] = 0, \quad (24)$$

from which we can introduce a scaled frequency $\tilde{\omega} = \omega \sqrt{\frac{b}{a}}$. Increasing the stiffness (a) or decreasing the density (b) of the base material will cause an overall shifting of the dispersion curves toward lower frequencies.

This is consistent with what is observed looking at the dispersion properties of a microstructured material's unit cell obtained via a Bloch–Floquet analysis. In the case for which $a = b$, the roots of equation (24) do not change at all. Thanks to this identification, we can now easily change the material constituting the unit cell (without changing the geometry) by scaling the material parameters accordingly without repeating the whole fitting process. In particular, all the cut-offs and asymptotes will be scaled by a quantity $\sqrt{\frac{a}{b}}$.

We explicitly remark again that scaling the macroscopic apparent density ρ of the unit cell by a factor $b > 0$ will change the frequency ω by the factor $\frac{1}{\sqrt{b}}$, i.e. the frequency is inversely proportional to the square root of the density of the unit cell. The wavenumber k is invariant under changing the macroscopic apparent density since the periodicity of the unit cell remains unaltered.

4.2. Consistency of the relaxed micromorphic model with respect to a change in the unit cell's size

While keeping the geometry and the material unaltered, the dispersion properties of a microstructured isotropic Cauchy material are inversely proportional to the size of its unit cell, meaning that halving the size of the unit cell will double the frequency response for each value of the length k of the wave vector, which also changes with the same inverse proportionality since it represents the spatial periodicity of the structure. This can be easily retrieved by performing standard Bloch–Floquet analysis.

In order to obtain this behavior with the relaxed micromorphic model, we must scale the elastic curvature tensors ($\mathbb{L}_s, \mathbb{L}_a$) and all the micro-inertia tensors ($\mathbb{J}_m, \mathbb{J}_c, \mathbb{T}_e, \mathbb{T}_c$) by the square of the size of the unit cell, and the micro-inertia curvature tensors ($\mathbb{M}_s, \mathbb{M}_a$) by the fourth power of the size of the unit cell.

To prove this, we consider a change in the size of the unit cell by some arbitrary factor $t > 0$, which requires the scaling of the characteristic length L_c (which is now considered to be equal to the size of the unit cell) by the same factor t . Assuming that all the other material parameters used remain constant, in equation (20) we substitute $L_c \rightarrow tL_c$ (see the coefficients in Appendices 2–4)

$$c_0 k^2 + t^2 c_1 k^4 - c_2 \omega^2 + t^2 c_3 k^2 \omega^2 + t^4 c_4 k^4 \omega^2 + t^2 c_5 \omega^4 + t^4 c_6 k^2 \omega^4 + t^6 c_7 k^4 \omega^4 - t^4 c_8 \omega^6 + t^6 c_9 k^2 \omega^6 + t^8 c_{10} k^4 \omega^6 = 0. \quad (25)$$

We can now collect $\frac{1}{t^2}$ in equation (25) arriving at

$$\frac{1}{t^2} [c_0 (tk)^2 + c_1 (tk)^4 - c_2 (t\omega)^2 + c_3 (tk)^2 (t\omega)^2 + c_4 (tk)^4 (t\omega)^2 + c_5 (t\omega)^4 + c_6 (tk)^2 (t\omega)^4 + c_7 (tk)^4 (t\omega)^4 - c_8 (t\omega)^6 + c_9 (tk)^2 (t\omega)^6 + c_{10} (tk)^4 (t\omega)^6] = 0. \quad (26)$$

It is clear to see from the comparison between equations (25) and (26) that their roots are simply linearly scaled with respect the factor t . This result enables the choice of having L_c equal to the size of the unit cell and thus allows us to change the latter in the microstructured material considered without needing to repeat the whole fitting procedure.

In particular, scaling the size L_c of the unit cell by the factor $t > 0$ will change the frequency ω and wavenumber k by the factor $\frac{1}{t}$, i.e. the frequency and wavenumber are reverse proportional to the size of the unit cell. This simple observation allows to perform the fitting procedure for the relaxed micromorphic model only once for each geometry of the unit cell: changing the size of the unit cell will result in an automatic fitting when

Table 2. Cut-off expressions for the pressure waves (left) and for the shear waves (right).

	0°	45°		0°	45°
Shear	$\omega_2 = \omega_{ss}$	$\omega_2 = \omega_s$	Pressure	$\omega_2 = \omega_s$	$\omega_2 = \omega_{ss}$
	$\omega_3 = \omega_r$	$\omega_3 = \omega_r$		$\omega_3 = \omega_p$	$\omega_3 = \omega_p$

Table 3. Numerical values of the asymptotes via Bloch–Floquet analysis using *Comsol Multiphysics*®.

	0°	45°		0°	45°
Shear	340.42 Hz	606.31 Hz	Pressure	581.95 Hz	689.20 Hz
	637.79 Hz	689.21 Hz		2040.81 Hz	1883.97 Hz
	2078.39 Hz	2375.78 Hz		2156.21 Hz	2376.45 Hz

suitably rescaling ω and k where none of the material parameters (except L_c) must be changed. Note that the slopes at the origin of the dispersion curves do not change when changing the size of the unit cell while keeping the geometry fixed.

4.3. Relaxed micromorphic cut-offs

The cut-offs of the dispersion curves play an important role in fitting the material parameters of the relaxed micromorphic model [51, 54, 57]. For the convenience of the reader, we show the calculations of the analytic expressions again. In the case $k = 0$, the dispersion relation (20) simplifies into

$$\begin{aligned}
 -c_2 \omega^2 + c_5 \omega^4 - c_8 \omega^6 = 0 &\iff \omega^2 \left(\omega^4 - \frac{c_5}{c_8} \omega^2 + \frac{c_2}{c_8} \right) = 0 \\
 \iff \omega_1^2 = 0, \quad \omega_{2,3}^2 = \frac{c_5 \pm \sqrt{c_5^2 - 4c_2c_8}}{2c_8}. & \quad (27)
 \end{aligned}$$

The coefficients c_2, c_5, c_8 depend on the elastic parameters $\mu_m, \kappa_m, \mu_m^*, \mu_c, \mu_e, \kappa_e, \mu_e^*$; the micro-inertia parameters $\kappa_\gamma, \gamma_1, \gamma_1^*, \gamma_2$; the macroscopic apparent density ρ ; and characteristic length L_c but are independent of the parameters for $\text{Curl } P, \nabla u$, and $\text{Curl } \dot{P}$, cf. Appendix 2.

Equations (27) can be simplified as in Table 2 with

$$\omega_r = \sqrt{\frac{\mu_c}{\rho L_c^2 \gamma_2}}, \quad \omega_s = \sqrt{\frac{\mu_e + \mu_m}{\rho L_c^2 \gamma_1}}, \quad \omega_{ss} = \sqrt{\frac{\mu_e^* + \mu_m^*}{\rho L_c^2 \gamma_1^*}}, \quad \omega_p = \sqrt{\frac{\kappa_e + \kappa_m}{\rho L_c^2 \kappa_\gamma}}. \quad (28)$$

We recognize that the expressions ω_s and ω_{ss} change from pressure to shear and shear to pressure, respectively, when going from 0° to 45° of incidence. Since the dispersion curves of the unit cell have two cut-offs that coincide, we chose them to be ω_s and ω_{ss} . Therefore, we introduce the following relation:

$$\omega_s = \omega_{ss} \iff \frac{\mu_e + \mu_m}{\gamma_1} = \frac{\mu_e^* + \mu_m^*}{\gamma_1^*}. \quad (29)$$

The values of these cut-offs have been fixed according to *Comsol Multiphysics*® simulations as

$$\omega_r = 554.61 \text{ Hz}, \quad \omega_s = \omega_{ss} = 2011.83 \text{ Hz}, \quad \omega_p = 2048.19 \text{ Hz}, \quad (30)$$

and the values of last points from *Comsol Multiphysics*® are used to fix the asymptotes, cf. Table 3.

5. Fitting of the relaxed micromorphic parameters: the particular case of vanishing curvature (without $\text{Curl } P$ and $\text{Curl } \dot{P}$)

In the numerical applications considered in this work, we start without considering the tensors $\mathbb{L}_s, \mathbb{L}_c$ and $\mathbb{M}_s, \mathbb{M}_c$, i.e. we neglect the effect of $\text{Curl } P$ and $\text{Curl } \dot{P}$ on the dynamic regime. This fundamentally changes

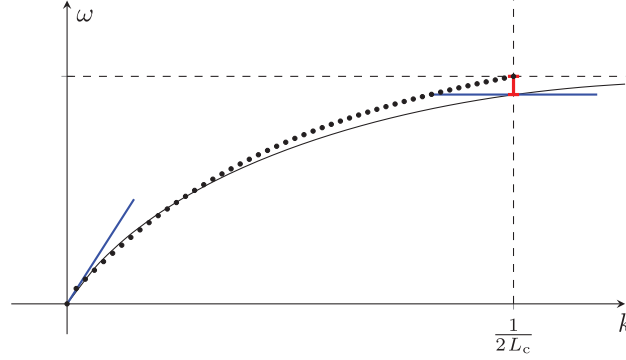


Figure 2. The fitting of the dispersion curves (black line) includes information about the slope at zero and the asymptotes (blue lines), while the remaining shape comes automatically. The Bloch–Floquet analysis used in *Comsol Multiphysics*[®] can only evaluate up to the periodicity limit $k = \frac{1}{2L_c}$ (black dots) which causes a slight gap between the dispersion curves at $k = \frac{1}{2L_c}$ and their corresponding asymptotes (red part).

the shape of the analytical expression (20) resulting in a new polynomial $p(k^2, \omega^2, \omega^4, \omega^6)$ with reduced order of k . Assuming that the wavenumber is always positive, we only have one single expression $k(\omega)$ describing all three dispersion curves:

$$c_0 k^2 - (c_2 + c_3^* k^2) \omega^2 + (c_5 + c_6^* k^2) \omega^4 - (c_8 + c_9^* k^2) \omega^6 = 0, \quad k = \omega \sqrt{\frac{c_2 - c_5 \omega^2 + c_8 \omega^4}{c_0 - c_3^* \omega^2 + c_6^* \omega^4 - c_9^* \omega^6}}. \quad (31)$$

The coefficients $c_0, c_2, c_3^*, c_5, c_6^*, c_8, c_9^*$ used⁹ have a different expression at 0° and 45° angle of incidence as well as for pressure and shear waves and are included in Appendix 2. The structure of $k(\omega)$ in equation (31)₂ can be also reported as a non-linear classic dispersion relation $k = \frac{\omega}{c_{p/s}(\omega)}$ with a frequency dependent group velocity $c_{p/s}$.

5.1. Asymptotes

Instead of fitting dispersion curves pointwise, we focus on using the analytical expression of the cut-offs ($k = 0$) and of the asymptotes ($k \rightarrow \infty$). The explicit expression of the cut-offs is already discussed in section 4.3. We use a similar approach to calculate the asymptotes as well by considering the limit $k \rightarrow \infty$ where only the terms with the highest order of k are important. Thus, we arrive at

$$c_0 - c_3^* \omega^2 + c_6^* \omega^4 - c_9^* \omega^6 = 0 \quad \Longleftrightarrow \quad \omega^6 - \frac{c_6^*}{c_9^*} \omega^4 + \frac{c_3^*}{c_9^*} \omega^2 - \frac{c_0}{c_9} = 0. \quad (32)$$

In contrast to the analytical expression of the cut-offs, we are not able to simplify the asymptotes' expression in a feasible way. This is mainly due to the fact that we must solve a third-order polynomial while we only had two non-zero cut-offs each before.

Since the dispersion curves of the unit cell obtained via Bloch–Floquet analysis are by nature periodic, the limit for $k \rightarrow \infty$ is per se meaningless when considering the Bloch–Floquet approach. The value for $k = \frac{1}{2L_c}$ (with L_c the size of the unit cell) is the periodicity limit. On the other hand, this limit has, of course, meaning for a continuum model like the relaxed micromorphic model. To reconcile these two limits in the fitting procedure, we will impose that the limit $k \rightarrow \infty$ for our continuum model will coincide with the periodicity limit of the Bloch–Floquet curves $k = \frac{1}{2L_c}$. This strategy allows us to preserve the width of the band gap, cf. Figure 2.

5.2. Fitting

We start the fitting with the macroscopic apparent density ρ and values of the macro parameters κ_M, μ_M, μ_M^* , i.e. the material constants necessary for the classical homogenization of an infinite large micromorphic material.

Table 4. Numerical values of the macroscopic apparent density ρ and the elastic macro-parameters κ_M, μ_M, μ_M^* for our unit cell when considering polyethylene as base material.

L_c	ρ	κ_M	μ_M	μ_M^*
(mm)	(kg/m ³)	(kPa)	(kPa)	(kPa)
20	361.2	352.2	200	99.36

Table 5. Dependence of the asymptotes of the dispersion curves on the free material parameters as function of the direction of propagation (0°/45°) and type of wave (shear/pressure).

	Pressure	Shear
0°	$\kappa_m, \bar{\kappa}_\gamma, \mu_m, \bar{\gamma}_1$	$\mu_c, \bar{\gamma}_2, \mu_m^*, \bar{\gamma}_1^*$
45°	$\kappa_m, \bar{\kappa}_\gamma, \mu_m^*, \bar{\gamma}_1^*$	$\mu_c, \bar{\gamma}_2, \mu_m, \bar{\gamma}_1$

For an anisotropic Cauchy material, the speed of the acoustic waves is

$$\begin{aligned}
 c_p &= \sqrt{\frac{\kappa_M + \mu_M}{\rho}}, & c_s &= \sqrt{\frac{\mu_M^*}{\rho}}, \\
 \bar{c}_p &= \sqrt{\frac{\kappa_M + \mu_M^*}{\rho}}, & \bar{c}_s &= \sqrt{\frac{\mu_M}{\rho}},
 \end{aligned} \tag{33}$$

where c_p, c_s are the speed of pressure and shear wave, respectively, for 0° of incidence, while \bar{c}_p, \bar{c}_s describe an incidence angle of 45°. For the tetragonal class of symmetry we choose, it holds

$$c_p^2 + c_s^2 = \frac{\kappa_M + \mu_M + \mu_M^*}{\rho} = \bar{c}_p^2 + \bar{c}_s^2, \tag{34}$$

reducing the system of equations to just three independent quantities. For the relaxed micromorphic model, we fit these macro parameters by the slope of the corresponding acoustic dispersion curves at $k = 0$

$$\mu_M = \bar{c}_s^2 \rho, \quad \mu_M^* = c_s^2 \rho, \quad \kappa_M = (c_p^2 - \bar{c}_s^2) \rho = (\bar{c}_p^2 - c_s^2) \rho. \tag{35}$$

The remaining unknown density ρ is given by the material and geometry of the cell we used (see Figure 1) and is directly computed as $\rho = \bar{\rho} \frac{A_{\text{total}} - A_{\text{voids}}}{A_{\text{total}}}$ with $\bar{\rho}$ as the density of polyethylene and $A_{\text{total}}, A_{\text{voids}}$ being the area of the whole cell and its voids, respectively. We list the numerical values in Table 4.

As a second step, we use the analytical expressions for the cut-offs (28) and calculate

$$\begin{aligned}
 \kappa_\gamma &= \frac{\kappa_e + \kappa_m}{\rho L_c^2 \omega_p^2}, & \gamma_1 &= \frac{\mu_e + \mu_m}{\rho L_c^2 \omega_s^2}, \\
 \gamma_1^* &= \frac{\mu_e^* + \mu_m^*}{\rho L_c^2 \omega_{ss}^2}, & \gamma_2 &= \frac{\mu_c}{\rho L_c^2 \omega_r^2}.
 \end{aligned} \tag{36}$$

Thus, we can reduce the system of independent variables by the four inertia parameters $\kappa_\gamma, \gamma_1, \gamma_1^*, \gamma_2$. Note again that we implied $\omega_s = \omega_{ss}$, see section 4.3.

As the third step, we use the analytic expression of the asymptotes for 0° and 45° resulting in 12 expressions in total which is more than the number of independent parameters remaining. Thus, we fit the last eight remaining parameters, namely the micro parameters $\kappa_m, \mu_m, \mu_m^*, \mu_c$ and inertia parameters $\bar{\kappa}_\gamma, \bar{\gamma}_1, \bar{\gamma}_1^*, \bar{\gamma}_2$, numerically, by minimizing the square error of the analytical expressions (32) and their corresponding numerical values from *Comsol Multiphysics*[®] (for $k = \frac{1}{2L_c}$ for 0° and $k = \frac{1}{\sqrt{2}L_c}$ for 45°). Thereby, we utilize the fact that each group of asymptotes only depend on four independent parameters to speed up the calculations, as summarized in Table 5.

Table 6. Obtained numerical values of the relaxed micromorphic model without curvature fitted for the metamaterial whose unit cell is given in Figure 1.

κ_m	μ_m	μ_m^*	μ_c	κ_e	μ_e	μ_e^*	
(kPa)	(kPa)	(kPa)	(kPa)	(kPa)	(kPa)	(kPa)	
546.0	286.9	175.04	15.24	992.8	664.4	229.9	
$\bar{\kappa}_\gamma$	$\bar{\gamma}_1$	$\bar{\gamma}_1^*$	$\bar{\gamma}_2$	κ_γ	γ_1	γ_1^*	γ_2
6.928	0.496	0.523	2.092	2.541	0.407	1.628	0.692

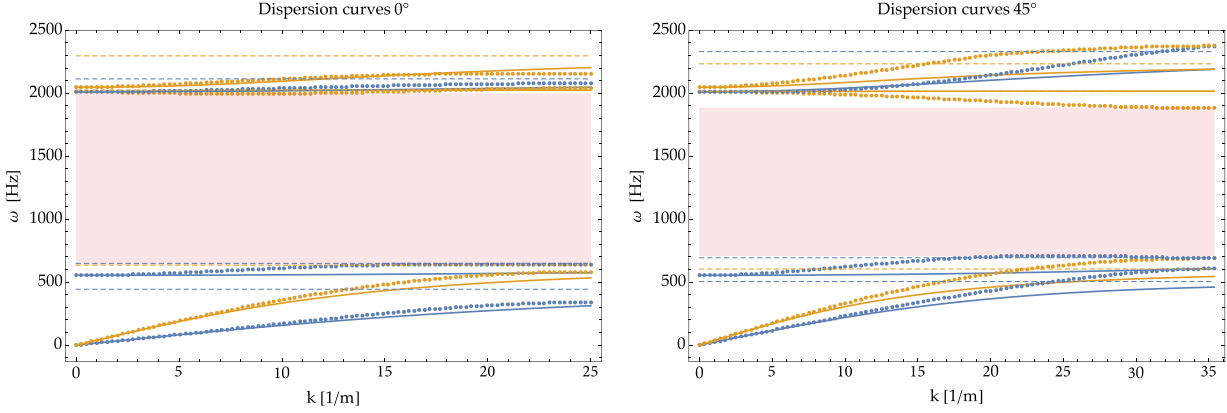


Figure 3. Dispersion curves $\omega(k)$ for 0° (left) and 45° (right) with pressure curves colored in yellow and shear in blue. The dots are the points computed with *Comsol Multiphysics*[®] while the smooth curves show the analytical expression of the dispersion curves for the relaxed micromorphic model without curvature, i.e. for $\alpha_1 = \beta_1 = 0$. The values of the curve's horizontal asymptotes are also shown with dashed lines.

We calculate these values with *Mathematica* using the *NMinimize*-algorithm with the inbuilt method *RandomSearch* running in a loop for multiple times. Here, we must start with reasonable initial values for all parameters involved. Note that it is always possible to imply $\mathbb{C}_{\text{micro}} = 2\mathbb{C}_{\text{macro}}$ as a conservative first guess implying

$$\mathbb{C}_e = \mathbb{C}_{\text{micro}} (\mathbb{C}_{\text{micro}} - \mathbb{C}_{\text{macro}})^{-1} \mathbb{C}_{\text{macro}} = 2\mathbb{C}_{\text{macro}} (2\mathbb{C}_{\text{macro}} - \mathbb{C}_{\text{macro}})^{-1} \mathbb{C}_{\text{macro}} = 2\mathbb{C}_{\text{macro}}, \quad (37)$$

i.e. simplifying the starting expressions¹⁰ by $\mathbb{C}_e = \mathbb{C}_{\text{micro}}$.

We list the numerical values of all parameters obtained via the fitting procedure presented in this section of the relaxed micromorphic model in Table 6.

5.3. Discussion

The fitting shown in Figure 3 behaves well for all frequencies ω and wavenumber k for 0° of incidence but loses some precision for an incidence angle of 45° especially for higher values of k . This calls for a further generalization of the relaxed micromorphic model which will be object of following papers. In any case, the achieved overall precision already allows us to explore the dispersive metamaterial's characteristics at a satisfactory level.

The absence of higher-order terms ($\text{Curl} P$ and $\text{Curl} \dot{P}$) caused the reduction to a single expression $k(\omega)$ describing all three dispersion curves in one, cf. equation (31). Thus, for every frequency ω , there is exactly one wavenumber k which may be imaginary if the term inside the root is negative. For the plots here, we only show $k(\omega)$ where the expression is real-valued and ignore imaginary $k(\omega)$ which arise in the band gap and for higher frequencies. Moreover, we cannot have two distinct wavenumbers with the same frequency which implies that all curves are monotonic. For every group of dispersion curves, e.g. the three pressure waves for 45° incidence, each individual curve is bounded by the others. Starting with the acoustic curves, their asymptote must be below the cut-off of the lower optic curve of the same type (pressure or shear), while the asymptote of the lower optic

curves is bounded from above by the cut-off of the highest optic curve. In particular, self-intersection between two pressure or two shear curves is not possible with this simplified version of the relaxed micromorphic model.

On the other hand, we observe that for the numerical values from *Comsol Multiphysics*[®] the asymptote of the acoustic shear wave at 45° should be slightly higher than the cut-off of the lower optic curve with 581.95 Hz and 554.61 Hz, respectively. In addition, assuming that all micro parameters κ_m, μ_m, μ_m^* (see Table 6) are larger than their corresponding macro counterparts κ_M, μ_M, μ_M^* , we did not manage to generate decreasing dispersion curves as observed for the lower optic pressure wave for an angle of incidence of 45°. This effect can instead be achieved when considering mixed space-time derivatives on the micro-distortion tensor P , cf. section 7.

When the relative positions of the curves allow to fit the cut-offs and the asymptotes of each curve separately (e.g. for an incidence angle of 0° shown here), the simplified version of the relaxed micromorphic model used does indeed show very good results. We want to emphasize that we only used the limit cases $k = 0$ (cut-offs) and $k \rightarrow \infty$ (asymptotes) for the fitting procedure but have an appreciable approximation for all values of k, ω .

6. Fitting of the relaxed micromorphic parameters with curvature (with Curl P)

To gain more freedom on the dispersion curves shape, we will now consider the addition of Curl P resulting in a higher-order polynomial in k which enables up to two distinct values of k for every $\omega \in \mathbb{R}_+$. At first, we still neglect Curl \dot{P} resulting in the slightly reduced characteristic polynomial

$$c_0 k^2 + c_1 k^4 - (c_2 + c_3 k^2 + c_4^* k^4) \omega^2 + (c_5 + c_6^* k^2 + c_7^* k^4) \omega^4 - (c_8 + c_9^* k^2) \omega^6 = 0. \quad (38)$$

The characteristic polynomial is of second order regarding k^2 which, assuming $k > 0$, results in two distinct roots

$$k_{1,2} = \frac{-c_0 + c_3 \omega^2 - c_6 \omega^4 - c_9^* \omega^6 \pm \sqrt{-4(c_1 + c_4^* \omega^2 + c_7 \omega^4)(-c_2 + c_5 \omega^4 + c_8 \omega^6) + (c_0 - c_3 \omega^2 + c_6^* \omega^4 + c_9 \omega^6)^2}}{2(c_1 + c_4^* \omega^2 + c_7^* \omega^4)} \quad (39)$$

describing the dispersion relation. The coefficients $c_0, c_1, c_2, c_3, c_4^*, c_5, c_6^*, c_7^*, c_8, c_9^*$ used¹¹ for the expression above change from 0° to 45° as well as for considering pressure and shear waves are included in the Appendix 3.

6.1. Asymptotes

Because the cut-offs are independent of the coefficients with higher order of k , they do not change with the addition of Curl P . Instead, the expressions of the asymptotes hugely differ compared to the expression without Curl P discussed before. We only include the terms with the highest order of k available and compute

$$\begin{aligned} c_1 - c_4^* \omega^2 + c_7^* \omega^4 = 0 & \iff \omega^4 - \frac{c_4^*}{c_7^*} \omega^2 + \frac{c_1}{c_7^*} = 0 \\ & \iff \omega_{1,2}^2 = \frac{c_4^* \pm \sqrt{(c_4^*)^2 - 4c_1 c_7^*}}{2c_7^*}. \end{aligned} \quad (40)$$

Surprisingly, the asymptotes with Curl P are significantly simpler because we must only solve a second-order polynomial instead of a third-order polynomial needed for the cut-offs and the asymptotes without Curl P . We now only have four distinct horizontal asymptotes (two shear and two pressure) in contrast to six before, which means that we must allow that the two curves (one shear and one pressure) will tend to infinity for high values of k , and our choice falls on the two highest optic curves. The same reasoning about the use of the asymptote in section 5.1 is applied here besides for the two highest optic curves that do not have a horizontal asymptote.

6.2. Fitting

The fitting procedure starts exactly as described in section 5.2. As a first step, we fit the macro parameters κ_M, μ_M, μ_M^* using the slopes of the dispersion curves for $k = 0$ which results in the same values as before. Following this, we express the micro-inertia $\kappa_\gamma, \gamma_1, \gamma_1^*, \gamma_2$ as a function of the numerical values of the cut-offs and the remaining independent material parameters. Overall, we arrive at four unknown micro parameters

Table 7. Dependence of the asymptotes of the dispersion curves on the free material parameters as function of the direction of propagation ($0^\circ/45^\circ$) and type of wave (shear/pressure).

	Pressure	Shear
0°	$\kappa_m, \bar{\kappa}_\gamma, \mu_m, \bar{\gamma}_1$	$\mu_c, \bar{\gamma}_2, \mu_m^*, \bar{\gamma}_1^*$
45°	$\kappa_m, \bar{\kappa}_\gamma, \mu_m^*, \bar{\gamma}_1^*$	$\mu_c, \bar{\gamma}_2, \mu_m, \bar{\gamma}_1$

Table 8. Numerical values of the relaxed micromorphic model with Curl P fitted for the metamaterial whose unit cell is given in Figure 1.

κ_m	μ_m	μ_m^*	μ_c	κ_e	μ_e	μ_e^*	α_1
(MPa)	(MPa)	(MPa)	(MPa)	(MPa)	(MPa)	(MPa)	(MPa)
1.674	20.04	8.748	15.33	4465	202.4	100.5	14.34
$\bar{\kappa}_\gamma$	$\bar{\gamma}_1$	$\bar{\gamma}_1^*$	$\bar{\gamma}_2$	κ_γ	γ_1	γ_1^*	γ_2
6.932	5.82	404.4	0.672	3.496	34.61	345	15.13

$\kappa_m, \mu_m, \mu_m^*, \mu_c$; four unknown inertia parameters $\bar{\kappa}_\gamma, \bar{\gamma}_1, \bar{\gamma}_1^*, \bar{\gamma}_2$; and the new elastic parameter α_1 belonging to Curl P .

Although the expressions of the asymptotes are different from the ones without the Curl P , we still have the same split between the parameters, resulting in four independent parameters for every group of asymptotes, cf. Table 7.

In particular, all eight expressions are independent on α_1 and thus Curl P . Hence, we have no analytic expressions to assign a value to this parameter. Note that the dispersion curves itself (in particular, their shape) still depend on α_1 but the cut-offs and asymptotes remain independent of this parameter. Because we miss the higher optic curves asymptotes, we introduce four new expressions as a replacement, by considering $k = \frac{1}{2L_c}$ at 0° and $\frac{1}{\sqrt{2}L_c}$ at 45° (instead of $k \rightarrow \infty$) for the corresponding curves, i.e. the highest value for k for which we still have numerical values using Bloch–Floquet analysis. Note again that L_c is always the size of the unit cell. These “pseudo-asymptotes” depend on the same parameters as their corresponding acoustic and lower optic curve asymptotes (cf. Table 7) and the additional independent parameter α_1 . The analytical expression is again too large to be included here but depend on all the coefficients c_0, \dots, c_9^* of the dispersion polynomial (38), cf. Appendix 3.

We list the numerical values of all parameters used for the fitting of the micromorphic model in Table 8.

6.3. Discussion

The fitting shown in Figure 4 including the curvature Curl P is worse compared to the one without, cf. Figure 3 and Table 8. This is mainly because we lost the higher optic curves asymptotes. Additionally, the shape of the curves which comes automatically by fitting all material parameters using only the cut-offs and asymptotes does not match properly with the data computed numerically with *Comsol Multiphysics*[®]. Most importantly, the fitting with Curl P shows the additional challenge of asymptotes that are approached at a very high wavenumber $k \gg \frac{1}{\sqrt{2}L_c}$ resulting in a poor fit for values of k between zero and the size of the unit cell, even if the slopes of the acoustic curves close to zero are well fitted. In particular, the acoustic shear wave is notably too slow at approaching its limit. Increasing α_1 substantially helps for lower frequencies but causes a much higher “pseudo-asymptote”, i.e. a worse fit for higher frequencies. To show this, we did a second fit only using the asymptotes of the acoustic and lower optic curves with α_1 as an independent parameter set by hand, cf. Figure 5.

Most other values remain at the same magnitude but are slightly higher, cf. Table 9. In future works, we will consider an enhanced relaxed micromorphic model to better describe these effects.

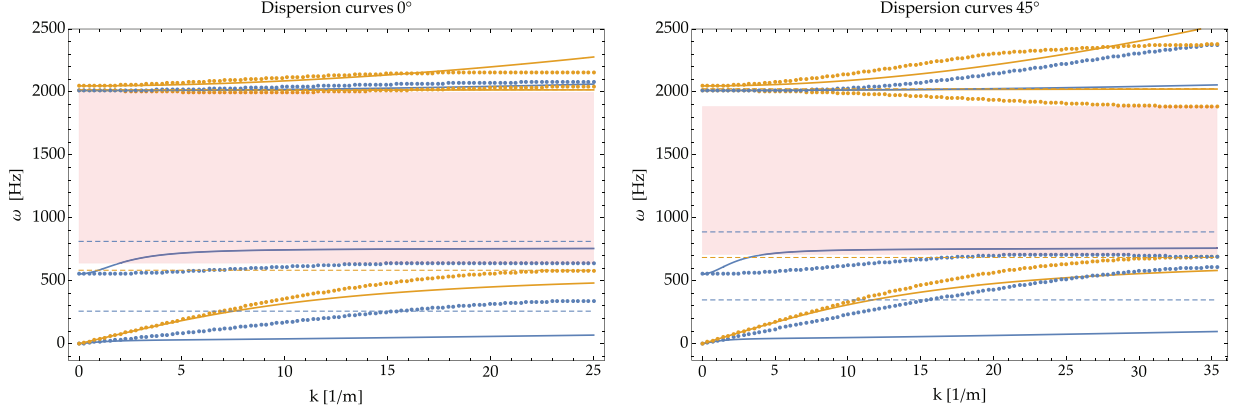


Figure 4. Dispersion curves $\omega(k)$ for 0° (left) and 45° (right) with pressure curves colored in yellow and shear in blue. The dots are the points computed with *Comsol Multiphysics*[®] while the smooth curves show the analytical expression of the dispersion curves for the relaxed micromorphic model for $\beta_1 = 0$. The values of the curve's horizontal asymptotes are also shown with dashed lines.

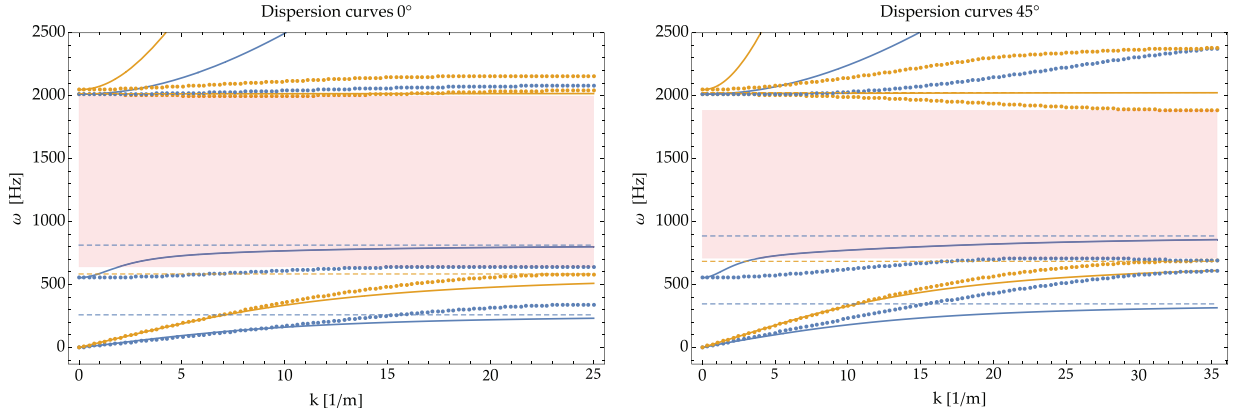


Figure 5. Dispersion curves $\omega(k)$ for 0° (left) and 45° (right) with pressure curves colored in yellow and shear in blue. The dots are the points computed with *Comsol Multiphysics*[®] while the smooth curves show the analytical expression of the dispersion curves for the relaxed micromorphic model for $\beta_1 = 0$. The values of the curve's horizontal asymptotes are also shown with dashed lines.

Table 9. Second set of alternative numerical values of the relaxed micromorphic model with $\text{Curl } P$ fitted for the metamaterial whose unit cell is given in Figure 1.

κ_m	μ_m	μ_m^*	μ_c	κ_e	μ_e	μ_e^*	α_1
(MPa)	(MPa)	(MPa)	(MPa)	(MPa)	(MPa)	(MPa)	(MPa)
1.418	20.04	8.936	15.61	468.4	202.4	100.5	240.0
$\bar{\kappa}_\gamma$	$\bar{\gamma}_1$	$\bar{\gamma}_1^*$	$\bar{\gamma}_2$	κ_γ	γ_1	γ_1^*	γ_2
3.616	9.552	408.0	4.288	3.116	34.61	351.2	15.45

7. Fitting of the relaxed micromorphic parameters with enhanced kinetic energy (with $\text{Curl } \dot{P}$)

We now include $\text{Curl } \dot{P}$ which reintroduces the third asymptote by considering the full dispersion polynomial

$$c_0 k^2 + c_1 k^4 - (c_2 + c_3 k^2 + c_4 k^4) \omega^2 + (c_5 + c_6 k^2 + c_7 k^4) \omega^4 - (c_8 + c_9 k^2 + c_{10} k^4) \omega^6 = 0, \quad (41)$$

with coefficients c_0, \dots, c_{10} depending on all the material parameters described before and β_1 belonging to $\text{Curl } \dot{P}$, cf. Appendix 4.

Table 10. Dependence of the asymptotes of the dispersion curves on the free material parameters as function of the direction of propagation ($0^\circ/45^\circ$) and type of wave (shear/pressure).

	Pressure	Shear
0°	$\kappa_m, \bar{\kappa}_\gamma, \mu_m, \bar{\gamma}_1$	$\mu_c, \bar{\gamma}_2, \mu_m^*, \bar{\gamma}_1^*$
45°	$\kappa_m, \bar{\kappa}_\gamma, \mu_m^*, \bar{\gamma}_1^*$	$\mu_c, \bar{\gamma}_2, \mu_m, \bar{\gamma}_1$
Superimposed	α_1, β_1	α_1, β_1

7.1. Asymptotes

Again, the cut-offs are independent on the coefficients with higher order of k and thus they do not change with respect to the two previous cases. For the asymptotes we only consider the terms with the highest order of k available and compute

$$c_1 - c_4\omega^2 + c_7\omega^4 - c_{10}\omega^6 = 0 \quad \Longleftrightarrow \quad \omega^6 - \frac{c_7}{c_{10}}\omega^4 + \frac{c_4}{c_{10}}\omega^2 - \frac{c_1}{c_{10}} = 0. \quad (42)$$

We have again three asymptotes (the roots of a third-order polynomial) which, in general, causes the analytical expressions to be impractical rather quickly. However, in this case, it is possible to find one root by hand

$$c_1 - c_4\omega^2 + c_7\omega^4 - c_{10}\omega^6 = 0 \quad \Longleftrightarrow \quad \left(1 - \rho L_c^2 \frac{\beta_1}{\alpha_1} \omega^2\right) (c_1 - c_4^*\omega^2 + c_7^*\omega^4) \quad (43)$$

with c_4^* and c_7^* from the dispersion relation (38) without $\text{Curl } \dot{P}$ which holds because

$$\rho L_c^2 \frac{\beta_1}{\alpha_1} c_1 = c_4 - c_4^* \quad \text{and} \quad \rho L_c^2 \frac{\beta_1}{\alpha_1} c_4^* = c_7 - c_7^* \quad \text{and} \quad \rho L_c^2 \frac{\beta_1}{\alpha_1} c_7^* = c_{10} \quad (44)$$

for all combinations of shear/pressure and $0^\circ/45^\circ$ angle of incidence. This is remarkable because it allows us to use the same analytical expressions for the acoustic and lower optic asymptotes from the calculations without $\text{Curl } \dot{P}$ of section 6, while the general expressions of the dispersion curves differ because of the addition of new terms. Second, the third asymptote

$$\omega_3 = \sqrt{\frac{\alpha_1}{\rho L_c^2 \beta_1}} \quad (45)$$

is identical for shear and pressure and invariant under change of angle of incidence. The same reasoning about the use of the asymptote in section 5.1 is applied here.

7.2. Fitting

The fitting starts as described in the sections before, using cut-offs and the slope of acoustic waves for $k = 0$ to reduce the number of independent parameters. Here we arrive at the same four unknown micro parameters $\kappa_m, \mu_m, \mu_m^*, \mu_c$ and four unknown inertia parameters $\bar{\kappa}_\gamma, \bar{\gamma}_1, \bar{\gamma}_1^*, \bar{\gamma}_2$ with the additional elastic parameter α_1, β_1 belonging to $\text{Curl } P$ and $\text{Curl } \dot{P}$, respectively. For the latter, we choose the acoustic pressure and lower optic shear curves as the one with the superimposed asymptote. The former are determined numerically using the remaining asymptotes (eight in total), see also Table 10.

However, because the analytical expression (45) of these four highest asymptotes is identical, while, in general, the numerical values from *Comsol Multiphysics*[®] can be distinct, we will arrive at the average of these four asymptotes. Moreover, we can only fix the ratio $\frac{\alpha_1}{\beta_1}$ which leaves us with one last free parameter, i.e. independent of the values of all cut-offs and asymptotes, which we fit by hand.

We list the numerical values of all parameters used in the micromorphic model in Table 11.

Table II. Numerical values for the relaxed micromorphic model with enhanced kinetic and potential energy terms ($\text{Curl } P$, $\text{Curl } \dot{P}$) for the metamaterial whose unit cell is given in Figure 1.

κ_m	μ_m	μ_m^*	μ_c	κ_e	μ_e	μ_e^*	α_1	
(MPa)	(kPa)	(kPa)	(kPa)	(kPa)	(kPa)	(kPa)	(Pa)	
35.22	228.4	27.67	110.7	355.8	1635	973.6	597.4	
$\bar{\kappa}_\gamma$	$\bar{\gamma}_1$	$\bar{\gamma}_1^*$	$\bar{\gamma}_2$	κ_γ	γ_1	γ_1^*	γ_2	β_1
1.168	2.004	2.276	0.820	58.68	3.188	1.184	1.856	$1.345 \cdot 10^{-2}$

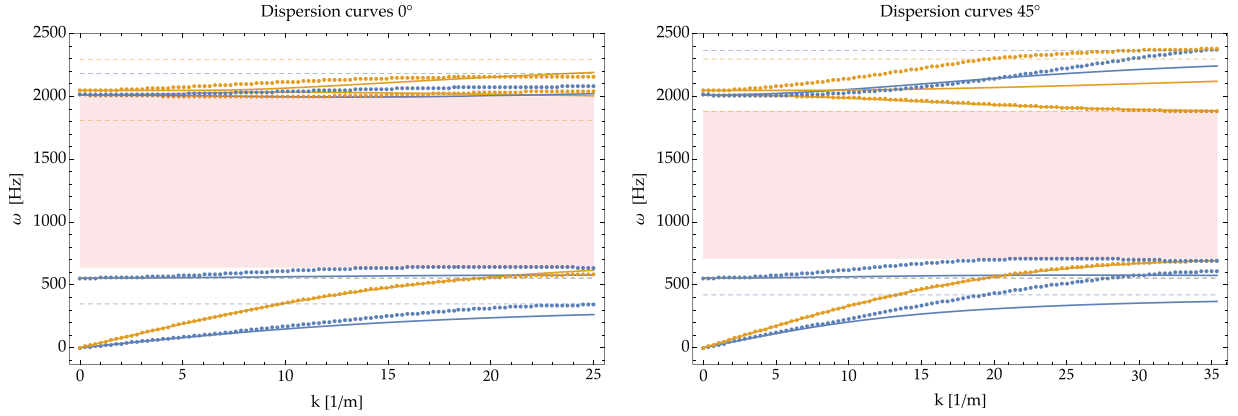


Figure 6. Dispersion curves $\omega(k)$ for 0° (left) and 45° (right) with pressure curves colored in yellow and shear in blue. The dots are the points computed with *Comsol Multiphysics*[®] while the smooth curves show the analytical expression of the dispersion curves for the relaxed micromorphic model. The values of the curve's horizontal asymptotes are also shown with dashed lines.

7.3. Discussion

The introduction of $\text{Curl } \dot{P}$ increases the quality of fitting again (see Figure 6) with the recovery of the higher optic curve asymptote, while the remaining free parameter α_1, β_1 can improve the shape of the curves. In particular, we can fit a dispersion curve with negative group velocity perfectly, the lower optic pressure curve for 45° , for the first time.

The fitting of the other curves is slightly worse compared to the calculations without curvature terms, and it is mainly due to the degenerated shape of $\text{Curl } \dot{P}$ and $\text{Curl } P$ in a plane problem, resulting in an isotropic behavior with only a single independent parameter. This causes four asymptotes to coincide.

We will not discuss in a fourth section the fitting with an enhanced kinetic energy with $\text{Curl } \dot{P}$ but without the curvature $\text{Curl } P$, since it leads to a degenerate dispersion polynomial $p(k, \omega)$ similar to the one described in section 6 resulting in only four configurable horizontal asymptotes for shear and pressure each. However, while we lost the higher optic asymptotes by adding $\text{Curl } P$ without $\text{Curl } \dot{P}$, the case with $\text{Curl } \dot{P}$ and without curvature $\text{Curl } P$ instead forces the limits of the one curve to zero as it can be seen as a limit case of expression (45), i.e. $\alpha_1 \rightarrow 0$.

8. Summary of the obtained results

Comparing the results of sections 5–7, the first approach which does not include $\text{Curl } P$ and $\text{Curl } \dot{P}$ shows the best agreement to the numerical values from *Comsol Multiphysics*[®] overall. At the same time, it must be noted that this simplified model without any curvature terms is only capable of describing monotonic dispersion curves with three disjointed domains for the three pressure waves and three disjointed domains for the three shear waves (crossing between pressure and shear waves is allowed, while it is not allowed between curves of the same type). The latter property can be easily deduced from equation (31)₂ which guarantees that for each value of ω there can only be one value of k .

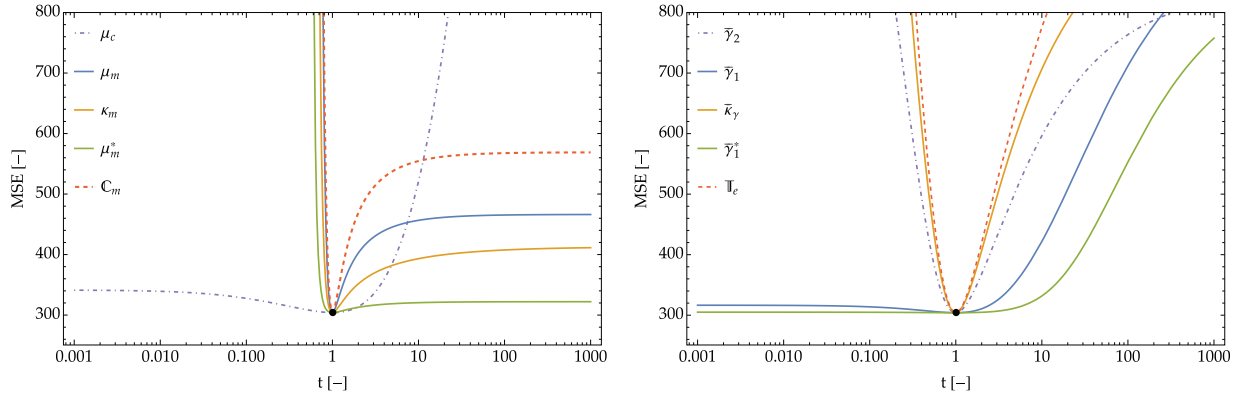


Figure 7. Mean squared error between the analytic expressions from the relaxed micromorphic model and their corresponding numerical values from *Comsol Multiphysics*[®] while changing the scaling coefficient t for different material parameters. Left: the static parameters $\kappa_m, \mu_m, \mu_m^*, \mu_c$ are colored in orange, blue, green, and purple, while the dashed red line shows the impact of scaling $\mathbb{C}_{\text{micro}}$ as a whole. Right: the dynamic parameters $\bar{\kappa}_\gamma, \bar{\gamma}_1, \bar{\gamma}_1^*, \bar{\gamma}_2$ are colored in orange, blue, green, and purple, while the dashed red line shows the impact of scaling \mathbb{T}_e as a whole.

In order to remove this constraint, the dispersion relation $p(k, \omega) = 0$ must contain higher order terms of the wavenumber k to allow the overlapping of the domains of curves of the same kind. To this aim, we started considering the full relaxed micromorphic model (with $\text{Curl } P$) and then augmented it with a new inertia term ($\text{Curl } \dot{P}$). The comparison of the analytic expression of the asymptotes with or without $\text{Curl } \dot{P}$ shown in equation (43) suggests that, when a new term is added to the elastic energy density, it is always better to include the corresponding dynamic part as well. In particular, considering $\text{Curl } P$ without its counterpart $\text{Curl } \dot{P}$ or vice versa causes missing terms in the dispersion polynomial $p(k, \omega) = 0$ resulting in fewer horizontal asymptotes.

While the model without curvature terms gives the best quantitative agreement (see Figure 3), the augmented relaxed micromorphic model still gives a good agreement and opens up the important possibility of decreasing modes with negative group velocity, cf. Figure 6. Note that $\text{Curl } P$ and $\text{Curl } \dot{P}$ degenerate for planar problems: for both terms, it just remains a single independent constitutive parameter (α_1 and β_1) restricting the class of symmetry for their constitutive tensors to the isotropic one.

We want to emphasize that the main focus of this work is not the result of the fitting of the three different approaches per se, but the semi-analytical fitting algorithm itself and the underlying consistency of the relaxed micromorphic model with respect to the material properties and some of the geometrical characteristic of the metamaterial that it represents. Using the complex but analytically defined expressions of the asymptotes, we can find a numerical fit of all material parameters by only giving the numerical values computed with *Comsol Multiphysics*[®] and the apparent mass density ρ of the unit cell. Note that we only use the cut-offs $k = 0$ and asymptotes $k \rightarrow \infty$ for calculating the material parameters while the shape of the curves for intermediate values of k comes automatically.

The routine is completely written with *Mathematica* allowing us to use symbolic calculations. The essential part of the fitting procedure uses the inbuilt algorithm *NMinimize* (with the Method *RandomSearch*) to minimize the mean square error of the asymptotes between the relaxed micromorphic model and the numerical values of the finite element approach in *Comsol Multiphysics*[®]. Therefore, in general, if a local minimum is found, it is not guaranteed that it corresponds to a global optimum as well.

In order to better understand the nature of the minimization problem, we visualize the impact of each parameter thanks to Figure 7 for the case without $\text{Curl } P$ and $\text{Curl } \dot{P}$ of section 5.2: given a set of material constants values, we move one parameter at the time and plot the impact on the error for the asymptotes.

It is crucial to state here that the expression of the coefficients shown in Appendices 2–4 are a priori constrained by the relations described in section 5.2 which reduces the number of independent parameters. This guarantees that the values of the cut-offs will not change if the micro parameters change because the corresponding micro-inertia parameters $\kappa_\gamma, \gamma_1, \gamma_1^*, \gamma_2$ are automatically scaled as well.

When considering the impact of the different independent parameters on the fitting error of the asymptotes, visible dissimilarity arises. While most coefficients show a simple behavior with one distinct minimum, the impact on the dispersion curves of the parameters μ_m^* and $\bar{\gamma}_1^*$ is very small. In addition to the numerical difficulty

caused by a vanishing gradient, it suggests finding additional quantities to constrain these material parameters, e.g. use a static test to fix μ_m^* beforehand. Overall, the minimum problem behaves remarkably well given its simple shape, which is in accordance with the fact that the fitting procedure always converges to very similar values of the parameters regardless of their initial guess.

9. Conclusion and perspectives

We presented an inertia-augmented relaxed micromorphic model that enhances the model proposed in [52–56] via the addition of a term $\text{Curl } \dot{P}$ in the kinetic energy. We then used this model to describe the dynamical behavior of a labyrinthine metamaterial and compared its predictability when setting all curvature terms to zero, when setting only $\text{Curl } \dot{P}$ to zero and when considering the full model (including $\text{Curl } P$ and $\text{Curl } \dot{P}$). The model's efficiency is tested by comparing the obtained dispersion curves to the ones issued via a standard Bloch–Floquet analysis. We find that the model without curvature terms gives the best average behavior (when considering the whole set of frequencies and wave numbers). However, this reduced model shows two main drawbacks: (1) it cannot give rise to curves with negative group velocity and (2) the horizontal asymptote of each curve is bounded by the cut-off of the following one. This implies a limitation of the fitting quality at higher wave numbers for some directions of propagation. To remove these constraints, the full model (including $\text{Curl } P$ and $\text{Curl } \dot{P}$) can be used. The fitting that we obtained with the full model remains of good quality (although precision is sometimes lowered point-wise) and we could perfectly describe (for the first time in a micromorphic framework) a higher-frequency mode with negative group velocity. The constraint concerning the asymptotes' boundedness is also removed in the full model, but a perfect fitting at higher wavenumbers cannot still be achieved due to a lack of extra microscopic degrees of freedom that are needed (at least for some directions) for a perfect fitting at wavelengths approaching the size of the unit cell.

We also tested the model's performances by considering only $\text{Curl } P$ and not $\text{Curl } \dot{P}$. The fitting quality is visibly worsening, thus suggesting that, when introducing a term in the strain energy, its dynamical counterpart in the kinetic energy should be always considered as well.

In addition to the fitting comparison presented in the present paper, one main result that we present here is the fitting procedure itself that has been automatized to a big extent by asking only the cut-offs and asymptotes to be imposed a priori. This has been done by imposing the exact value of the cut-offs and minimizing the asymptotes' mean square error compared to the exact numerical values issued via Bloch–Floquet analysis. The rest of the curves' fitting follows directly.

The routine for the fitting procedure is written with *Mathematica* allowing us to use symbolic calculations. The essential part of the routine uses the built-in algorithm *NMinimize* (with the Method *RandomSearch*) to minimize the asymptote's mean square error. We finally checked whether the found local minimum is also a global minimum. We found that all the elastic parameters achieve a global minimum in the computed configuration, but μ_m^* and $\bar{\gamma}_1^*$ seem to have little effect on the overall fitting after a certain threshold. This result seems to suggest that the values of these parameters should be eventually fixed beforehand with the help of extra independent static and/or dynamic tests.

Based on the findings of this paper, we will briefly present some insight that will give directions to the follow-up research:


- Further enhance the relaxed micromorphic model via the addition of extra microscopic degrees of freedom to increase its precision at very small wavelengths (approaching the unit cell's size);
- Design complex large-scale meta-structures that control elastic energy using the new labyrinthine metamaterial as a basic building block. This design would not be otherwise possible due to the huge number of degrees of freedom resulting from the meshing of all the tiny elements contained in the labyrinthine unit cells;
- Study negative refraction phenomena in meta-structures including the new labyrinthine metamaterial as a basic building block;
- Design complex structures for wave control simultaneously including the different metamaterials that were characterized via the relaxed micromorphic model until now.

Funding

The author(s) disclosed receipt of the following financial support for the research, authorship, and/or publication of this article: Angela Madeo, Gianluca Rizzi, and Jendrik Voss acknowledge support from the European Commission through the funding of the ERC Consolidator Grant META-LEGO, N° 101001759. Angela Madeo and Gianluca Rizzi acknowledge funding from the French Research Agency ANR, “METASmart” (ANR-17CE08-0006). Patrizio Neff acknowledges support in the framework of the DFG-Priority Programme 2256 “Variational Methods for Predicting Complex Phenomena in Engineering Structures and Materials”, Neff 902/10-1, Project-No. 440935806.

ORCID iDs

Jendrik Voss  <https://orcid.org/0000-0001-8912-9625>

Gianluca Rizzi  <https://orcid.org/0000-0002-5967-5403>

Notes

1. Here we target a complete expression of the Lagrangian that was not considered in literature [52–55] to show the effect on the predictability of the dispersion curves provided by each term.
2. The tensors \mathbb{J}_m , \mathbb{T}_e , \mathbb{C}_e , $\mathbb{C}_{\text{micro}}$, \mathbb{L}_s and \mathbb{M}_s have a minor symmetry ($\mathbb{A}_{(ij)(kl)} = \mathbb{A}_{(ji)(kl)} = \mathbb{A}_{(ij)(lk)} = \mathbb{A}_{(ji)(lk)}$), while \mathbb{J}_c , \mathbb{T}_c , \mathbb{C}_c , \mathbb{L}_a , and \mathbb{M}_a have a minor anti-symmetry ($\mathbb{B}_{[ij][kl]} = -\mathbb{B}_{[ji][kl]}$, $\mathbb{B}_{[ij][kl]} = -\mathbb{B}_{[ij][lk]}$, $\mathbb{B}_{[ij][kl]} = \mathbb{B}_{[ji][lk]}$), for instance, we can write $\langle \mathbb{J}_m \text{sym } \dot{P}, \text{sym } \dot{P} \rangle + \langle \mathbb{J}_c \text{skew } \dot{P}, \text{skew } \dot{P} \rangle = \langle (\mathbb{J}_m + \mathbb{J}_c) \dot{P}, \dot{P} \rangle$.
3. The dimensions of the matrix representation of elastic and micro-inertia tensors are $(\mathbb{C}_e, \mathbb{C}_{\text{micro}}, \mathbb{J}_m, \mathbb{T}_e, \mathbb{L}_s, \mathbb{M}_s) \in \mathbb{R}^{6 \times 6}$ and $(\mathbb{C}_c, \mathbb{J}_c, \mathbb{T}_c, \mathbb{L}_a, \mathbb{M}_a) \in \mathbb{R}^{3 \times 3}$. In the previous works [51,55,57], the parameters in \mathbb{J}_m and \mathbb{J}_c were referred as η_i or ρL_i^2 , and the parameters in \mathbb{T}_e , \mathbb{T}_c as $\bar{\eta}_i$ or $\rho \bar{L}_i^2$.
4. We retain the plane strain hypothesis in the remainder of the paper.
5. We write “ m ” for “*micro*” and “ M ” for “*macro*” for the corresponding elastic parameters to shorten the following expressions.
6. The components of u and P depend only on $\{x_1, x_2\}$ and $u_3 = P_{13} = P_{31} = P_{23} = P_{32} = P_{33} = 0$.
7. It is remarked that this is only possible since the condition (12) is satisfied.
8. Scaling the density ρ automatically scale all the micro-inertia terms too since all of them are already proportional to it.
9. The notation c_i^* throughout the following sections indicates that enhancing the model, i.e. reintroducing the neglected tensors for $\text{Curl } P$ and $\text{Curl } \dot{P}$, changes c_i^* by the addition of new terms. In contrast, the notation c_i without an asterisk indicates that the coefficient is complete in the sense that it remains unchanged when including $\text{Curl } P$ and $\text{Curl } \dot{P}$ as well.
10. Even though the name of the elastic tensors (micro-, meso-, macro-) suggests that the values of \mathbb{C}_e should be bounded by $\mathbb{C}_{\text{micro}}$ from above and $\mathbb{C}_{\text{macro}}$ from below, this is not the case in general. For a very simple unit cell whose structure differs little from the homogeneous cell, $\mathbb{C}_{\text{micro}}$ is very similar to $\mathbb{C}_{\text{macro}}$ implying that $\mathbb{C}_e = \mathbb{C}_{\text{micro}} (\mathbb{C}_{\text{micro}} - \mathbb{C}_{\text{macro}})^{-1} \mathbb{C}_{\text{macro}}$ tends to infinity. Thus, \mathbb{C}_e is not an elastic tensor in the classical sense and very large values impose $\text{sym } P \approx \text{sym } \nabla u$.
11. The notation c_i^* still indicates that the coefficient is missing components belonging to the neglected tensor for $\text{Curl } \dot{P}$, while c_i without an asterisk states that the coefficient is the same of the enhanced relaxed micromorphic model with $\text{Curl } \dot{P}$.

References

- [1] Lakes, R. Foam structures with a negative Poisson’s ratio. *Science* 1987; 235(4792): 1038–1040.
- [2] Frenzel, T, Kadic, M, and Wegener, M. Three-dimensional mechanical metamaterials with a twist. *Science* 2017; 358(6366): 1072–1074.
- [3] Rizzi, G, Dal Corso, F, Veber, D, et al. Identification of second-gradient elastic materials from planar hexagonal lattices. Part II: mechanical characteristics and model validation. *Int J Solids Struct* 2019; 176(1): 19–35.
- [4] Liu, Z, Zhang, X, Mao, Y, et al. Locally resonant sonic materials. *Science* 2000; 289(5485): 1734–1736.
- [5] Wang, P, Casadei, F, Shan, S, et al. Harnessing buckling to design tunable locally resonant acoustic metamaterials. *Phys Rev Lett* 2014; 113(1): 014301.
- [6] Bilal, OR, Ballagi, D, and Daraio, C. Architected lattices for simultaneous broadband attenuation of airborne sound and mechanical vibrations in all directions. *Phys Rev Appl* 2018; 10(5): 054060.
- [7] Celli, P, Yousefzadeh, B, Daraio, C, et al. Bandgap widening by disorder in rainbow metamaterials. *Appl Phys Lett* 2019; 114(9): 091903.
- [8] Bückmann, T, Kadic, M, Schittny, R, et al. Mechanical cloak design by direct lattice transformation. *Proc Natl Acad Sci* 2015; 112(16): 4930–4934.
- [9] Misseroni, D, Colquitt, DJ, Movchan, AB, et al. Cymatics for the cloaking of flexural vibrations in a structured plate. *Sci Rep* 2016; 6(1): 1–11.

- [10] Guenneau, S, Movchan, A, Pétursson, G, et al. Acoustic metamaterials for sound focusing and confinement. *New J Phys* 2007; 9(11): 399.
- [11] Cummer, SA, Christensen, J, and Alú, A. Controlling sound with acoustic metamaterials. *Nat Rev Mater* 2016; 1(3): 1–13.
- [12] Kaina, N, Causier, A, Bourlier, Y, et al. Slow waves in locally resonant metamaterials line defect waveguides. *Sci Rep* 2017; 7(1): 1–11.
- [13] Tallarico, D, Trevisan, A, Movchan, NV, et al. Edge waves and localization in lattices containing tilted resonators. *Front Mater* 2017; 4(1): 16.
- [14] Zhu, R, Liu, XN, Hu, GK, et al. Negative refraction of elastic waves at the deep-subwavelength scale in a single-phase metamaterial. *Nat Commun* 2014; 5(1): 5510.
- [15] Kaina, N, Lemoult, F, Fink, M, et al. Negative refractive index and acoustic superlens from multiple scattering in single negative metamaterials. *Nature* 2015; 525(7567): 77–81.
- [16] Willis, JR. Negative refraction in a laminate. *J Mech Phys Solids* 2016; 97: 10–18.
- [17] Krushynska, A, Bosia, F, Miniaci, M, et al. Spider web-structured labyrinthine acoustic metamaterials for low-frequency sound control. *New J Phys* 2017; 19(10): 105001.
- [18] Krushynska, AO, Bosia, F, and Pugno, NM. Labyrinthine acoustic metamaterials with space-coiling channels for low-frequency sound control. *Acta Acust United Ac* 2018; 104(2): 200–210.
- [19] Xie, Y, Konneker, A, Popa, BI, et al. Tapered labyrinthine acoustic metamaterials for broadband impedance matching. *Appl Phys Lett* 2013; 103(20): 201906.
- [20] Kumar, S, and Lee, HP. Labyrinthine acoustic metastructures enabling broadband sound absorption and ventilation. *Appl Phys Lett* 2020; 116(13): 134103.
- [21] Frenzel, T, David Brehm, J, Bückmann, T, et al. Three-dimensional labyrinthine acoustic metamaterials. *Appl Phys Lett* 2013; 103(6): 061907.
- [22] Liu, J, Li, L, Xia, B, et al. Fractal labyrinthine acoustic metamaterial in planar lattices. *Int J Solids Struct* 2018; 132(1): 20–30.
- [23] Bensoussan, A, Lions, J, and Papanicolaou, G. *Asymptotic analysis for periodic structures*, vol. 374. Providence, RI: American Mathematical Society, 2011.
- [24] Suquet, P. Elements of homogenization for inelastic solid mechanics, homogenization techniques for composite media. *Lect Notes Phys* 1985; 272(1): 193.
- [25] Miehe, C, Schröder, J, and Schotte, J. Computational homogenization analysis in finite plasticity simulation of texture development in polycrystalline materials. *Comput Method Appl M* 1999; 171(3-4): 387–418.
- [26] Geers, M, Kouznetsova, V, and Brekelmans, M. Multi-scale computational homogenization: trends and challenges. *J Comput Appl Math* 2010; 234(7): 2175–2182.
- [27] Hill, R. Elastic properties of reinforced solids: some theoretical principles. *J Mech Phys Solids* 1963; 11(5): 357–372.
- [28] Sánchez-Palencia, E. Non-homogeneous media and vibration theory. *Lect Notes Phys* 1980; 127.
- [29] Allaire, G. Homogenization and two-scale convergence. *SIAM J Math Anal* 1992; 23(6): 1482–1518.
- [30] Milton, G. *The theory of composites* (Cambridge Monographs on Applied and Computational Mathematics). Cambridge: Cambridge University Press, 2002.
- [31] Hashin, Z, and Shtrikman, S. A variational approach to the theory of the elastic behaviour of multiphase materials. *J Mech Phys Solids* 1963; 11(2): 127–140.
- [32] Willis, J. Bounds and self-consistent estimates for the overall properties of anisotropic composites. *J Mech Phys Solids* 1977; 25(3): 185–202.
- [33] Pideri, C, and Seppecher, P. A second gradient material resulting from the homogenization of an heterogeneous linear elastic medium. *Continuum Mech Therm* 1997; 9(5): 241–257.
- [34] Bouchitté, G, and Bellieud, M. Homogenization of a soft elastic material reinforced by fibers. *Asymptotic Anal* 2002; 32(2): 153–183.
- [35] Camar-Eddine, M, and Seppecher, P. Determination of the closure of the set of elasticity functionals. *Arch Ration Mech An* 2003; 170(3): 211–245.
- [36] Bacigalupo, A, and Gambarotta, L. Second-gradient homogenized model for wave propagation in heterogeneous periodic media. *Int J Solids Struct* 2014; 51(5): 1052–1065.
- [37] Srivastava, A, and Nemat-Nasser, S. On the limit and applicability of dynamic homogenization. *Wave Motion* 2014; 51(7): 1045–1054.
- [38] Sridhar, A, Kouznetsova, V, and Geers, M. A general multiscale framework for the emergent effective elastodynamics of metamaterials. *J Mech Phys Solids* 2018; 111(1): 414–433.
- [39] Srivastava, A, and Willis, JR. Evanescent wave boundary layers in metamaterials and sidestepping them through a variational approach. *P Roy Soc A: Math Phys* 2017; 473(2200): 20160765.
- [40] Chen, W, and Fish, J. A dispersive model for wave propagation in periodic heterogeneous media based on homogenization with multiple spatial and temporal scales. *J Appl Mech* 2001; 68(2): 153–161.
- [41] Boutin, C, Rallu, A, and Hans, S. Large scale modulation of high frequency waves in periodic elastic composites. *J Mech Phys Solids* 2014; 70(1): 362–381.
- [42] Craster, R, Kaplunov, J, and Pichugin, A. High-frequency homogenization for periodic media. *P Roy Soc A: Math Phys* 2010; 466(2120): 2341–2362.

- [43] Andrianov, I, Bolshakov, V, Danishevskiy, V, et al. Higher order asymptotic homogenization and wave propagation in periodic composite materials. *P Roy Soc A: Math Phys* 2008; 464(2093): 1181–1201.
- [44] Hu, R, and Oskay, C. Nonlocal homogenization model for wave dispersion and attenuation in elastic and viscoelastic periodic layered media. *J Appl Mech* 2017; 84(3): 031003.
- [45] Willis, J. Exact effective relations for dynamics of a laminated body. *Mech Mater* 2009; 41(4): 385–393.
- [46] Willis, J. Effective constitutive relations for waves in composites and metamaterials. *P Roy Soc A: Math Phys* 2011; 467(2131): 1865–1879.
- [47] Willis, J. The construction of effective relations for waves in a composite. *CR Mécanique* 2012; 340(4-5): 181–192.
- [48] Krushynska, AO, Miniaci, M, Bosia, F, et al. Coupling local resonance with Bragg band gaps in single-phase mechanical metamaterials. *Extrem Mech Lett* 2017; 12(1): 30–36.
- [49] Neff, P, Ghiba, ID, Madeo, A, et al. A unifying perspective: the relaxed linear micromorphic continuum. *Continuum Mech Therm* 2014; 26(5): 639–681.
- [50] Neff, P, Ghiba, ID, Lazar, M, et al. The relaxed linear micromorphic continuum: well-posedness of the static problem and relations to the gauge theory of dislocations. *Q J Mech Appl Math* 2015; 68(1): 53–84.
- [51] d’Agostino, MV, Barbagallo, G, Ghiba, ID, et al. Effective description of anisotropic wave dispersion in mechanical band-gap metamaterials via the relaxed micromorphic model. *J Elasticity* 2020; 139(2): 299–329.
- [52] Aivaliotis, A, Daouadji, A, Barbagallo, G, et al. Microstructure-related Stoneley waves and their effect on the scattering properties of a 2D Cauchy/relaxed-micromorphic interface. *Wave Motion* 2019; 90(1): 99–120.
- [53] Aivaliotis, A, Tallarico, D, d’Agostino, MV, et al. Frequency- and angle-dependent scattering of a finite-sized meta-structure via the relaxed micromorphic model. *Arch Appl Mech* 2020; 90(5): 1073–1096.
- [54] Rizzi, G, Collet, M, Demore, F, et al. Exploring metamaterials’ structures through the relaxed micromorphic model: switching an acoustic screen into an acoustic absorber. *Front Mater* 2021; 7(1): 589701.
- [55] Rizzi, G, d’Agostino, MV, Neff, P, et al. Boundary and interface conditions in the relaxed micromorphic model: exploring finite-size metastructures for elastic wave control. *Math Mech Solids* 2022; 27(6): 1053–1068.
- [56] Rizzi, G, Neff, P, and Madeo, A. Metamaterial shields for inner protection and outer tuning through a relaxed micromorphic approach. arXiv preprint arXiv:2111.12001, 2021.
- [57] Neff, P, Eidel, B, d’Agostino, MV, et al. Identification of scale-independent material parameters in the relaxed micromorphic model through model-adapted first order homogenization. *J Elasticity* 2020; 139(2): 269–298.
- [58] Bernstein, DS. *Matrix mathematics: theory, facts, and formulas*. 2nd ed. Princeton, NJ: Princeton University Press, 2009.

Appendix I

Most general fourth-order tensor belonging to the tetragonal symmetry class

Considering the following quadratic form

$$Y = \langle \mathbb{L}D, D \rangle, \quad (46)$$

where \mathbb{L} is a fourth-order tensor and D is a second-order one, the most general form of \mathbb{L} , if it belongs to the tetragonal symmetry class written in Voigt notation, is

$$L = \begin{pmatrix} l_1 & l_5 & l_6 & 0 & 0 & 0 & 0 & 0 & 0 \\ l_5 & l_1 & l_6 & 0 & 0 & 0 & 0 & 0 & 0 \\ l_6 & l_6 & l_2 & 0 & 0 & 0 & 0 & 0 & 0 \\ 0 & 0 & 0 & l_3 + l_7 + l_9 & l_3 - l_7 & 0 & 0 & 0 & 0 \\ 0 & 0 & 0 & l_3 - l_7 & l_3 + l_7 - l_9 & 0 & 0 & 0 & 0 \\ 0 & 0 & 0 & 0 & 0 & l_3 + l_7 + l_9 & l_3 - l_7 & 0 & 0 \\ 0 & 0 & 0 & 0 & 0 & l_3 - l_7 & l_3 + l_7 - l_9 & 0 & 0 \\ 0 & 0 & 0 & 0 & 0 & 0 & 0 & l_4 + l_8 & l_4 - l_8 \\ 0 & 0 & 0 & 0 & 0 & 0 & 0 & l_4 - l_8 & l_4 + l_8 \end{pmatrix}, \quad (47)$$

where the order of the element of the vector associated with the quadratic form 46 is

$$d = (D_{11}, D_{22}, D_{33}, D_{23}, D_{32}, D_{13}, D_{31}, D_{12}, D_{21})^T. \quad (48)$$

If we now split the tensor D in its symmetric and skew-symmetric part, the corresponding vector in Voigt notation is

$$d_s = (D_{11}, D_{22}, D_{33}, D_{23} + D_{32}, D_{13} + D_{31}, D_{12} + D_{21})^T, \quad d_a = \frac{1}{2} (D_{23} - D_{32}, D_{13} - D_{31}, D_{12} - D_{21})^T. \quad (49)$$

Because of the class of symmetry considered, it is necessary to take into account a mixed constitutive matrix that couples the symmetric and skew-symmetric part of D in order to build back the quadratic form Y

$$Y = \langle \mathbb{L}D, D \rangle = \langle Ld, d \rangle = \langle L_s d_s, d_s \rangle + \langle L_a d_a, d_a \rangle + 2 \langle L_{\text{mix}} d_s, d_a \rangle \quad (50)$$

where

$$L_s = \begin{pmatrix} \ell_1 & \ell_5 & \ell_6 & 0 & 0 & 0 \\ \ell_5 & \ell_1 & \ell_6 & 0 & 0 & 0 \\ \ell_6 & \ell_6 & \ell_2 & 0 & 0 & 0 \\ 0 & 0 & 0 & \ell_3 & 0 & 0 \\ 0 & 0 & 0 & 0 & \ell_3 & 0 \\ 0 & 0 & 0 & 0 & 0 & \ell_4 \end{pmatrix}, \quad L_a = \begin{pmatrix} 4\ell_7 & 0 & 0 \\ 0 & 4\ell_7 & 0 \\ 0 & 0 & 4\ell_8 \end{pmatrix}, \quad L_{\text{mix}} = \begin{pmatrix} 0 & 0 & 0 & \ell_9 & 0 & 0 \\ 0 & 0 & 0 & 0 & \ell_9 & 0 \\ 0 & 0 & 0 & 0 & 0 & 0 \end{pmatrix}. \quad (51)$$

Only the coefficient ℓ_9 couples the symmetric and skew-symmetric part of D , and it produces works just for out-of-plane deformation if a plane strain problem ($x_1 O x_2$) is considered, which means that it is not involved in the constitutive relations for both the gradient of the displacement ∇u and the micro-distortion tensor P , while it is for the $\text{Curl} P$ or for $\text{Curl} \dot{P}$. Nevertheless, the quadratic form Y when $D = \text{Curl} P$ (see equation (11)) under a plane strain hypothesis is

$$Y = (\ell_3 + \ell_7 + \ell_9) ((\text{Curl} P)_{13}^2 + (\text{Curl} P)_{23}^2) \quad (52)$$

which depends on just one cumulative coefficient. This makes the coupling coefficient ℓ_9 and the skew-symmetric coefficient ℓ_7 redundant.

Appendix 2

Coefficients for the dispersion curves without Curl P

For the relaxed micromorphic model without curvature, we arrived equation (31) at the dispersion polynomial

$$c_0 k^2 - (c_2 + c_3^* k^2) \omega^2 + (c_5 + c_6^* k^2) \omega^4 - (c_8 + c_9^* k^2) \omega^6 \quad (53)$$

We list the coefficients $(c_0, c_2, c_3^*, c_5, c_6^*, c_8, c_9^*)^T$.

$$\begin{pmatrix} 4(\mu_e \kappa_m \mu_m + \kappa_e (\kappa_m (\mu_e + \mu_m) + \mu_e \mu_m)) \\ 4\rho (\kappa_e + \kappa_m) (\mu_e + \mu_m) \\ 4\rho L_c^2 ((\bar{\kappa}_\gamma + \bar{\gamma}_1) (\kappa_e + \kappa_m) (\mu_e + \mu_m) + \gamma_1 (\mu_e \kappa_m + \kappa_e (\mu_e + \kappa_m)) + \kappa_\gamma (\kappa_e (\mu_e + \mu_m) + \mu_e \mu_m)) \\ 4\rho^2 L_c^2 (\kappa_\gamma (\mu_e + \mu_m) + \gamma_1 (\kappa_e + \kappa_m)) \\ 4\rho^2 L_c^4 (\kappa_\gamma (\bar{\kappa}_\gamma + \bar{\gamma}_1) (\mu_e + \mu_m) + \gamma_1 ((\bar{\kappa}_\gamma + \bar{\gamma}_1) (\kappa_e + \kappa_m) + \kappa_\gamma (\kappa_e + \mu_e))) \\ 4\gamma_1 \rho^3 L_c^4 \kappa_\gamma \\ 4\gamma_1 \rho^3 L_c^6 \kappa_\gamma (\bar{\kappa}_\gamma + \bar{\gamma}_1) \end{pmatrix} \quad (54)$$

Shear 0° :

$$\begin{pmatrix} 4\mu_c \mu_e^* \mu_m^* \\ 4\rho \mu_c (\mu_e^* + \mu_m^*) \\ 4\rho L_c^2 (\mu_c (\bar{\gamma}_2 (\mu_e^* + \mu_m^*) + \bar{\gamma}_1^* (\mu_e^* + \mu_m^*) + \gamma_1^* \mu_e^*) + \gamma_2 (\mu_c (\mu_e^* + \mu_m^*) + \mu_e^* \mu_m^*)) \\ 4\rho^2 L_c^2 (\mu_c \gamma_1^* + \gamma_2 (\mu_e^* + \mu_m^*)) \\ 4\rho^2 L_c^4 (\bar{\gamma}_2 \mu_c \gamma_1^* + \mu_c \gamma_1^* \bar{\gamma}_1^* + \gamma_2 \bar{\gamma}_2 (\mu_e^* + \mu_m^*) + \gamma_2 \bar{\gamma}_1^* (\mu_e^* + \mu_m^*) + \gamma_2 \gamma_1^* (\mu_e^* + \mu_c)) \\ 4\gamma_2 \rho^3 L_c^4 \gamma_1^* \\ 4\gamma_2 \rho^3 L_c^6 \gamma_1^* (\bar{\gamma}_1^* + \bar{\gamma}_2) \end{pmatrix} \quad (55)$$

Pressure 45° :

$$\left(\begin{array}{c} 4(\kappa_m \mu_e^* \mu_m^* + \kappa_e(\mu_e^* + \mu_m^*) + \mu_e^* \mu_m^*) \\ 4\rho(\kappa_e + \kappa_m)(\mu_e^* + \mu_m^*) \\ 4L_c^2 \rho((\kappa_e + \kappa_m)(\gamma_1^* \mu_e^* + \bar{\gamma}_1^*(\mu_e^* + \mu_m^*) + \bar{\kappa}_\gamma \mu_e^* + \bar{\kappa}_\gamma \mu_m^*) + \gamma_1^* \kappa_e \kappa_m + \kappa_\gamma \mu_e^* \mu_m^* + \kappa_\gamma \kappa_e(\mu_e^* + \mu_m^*)) \\ 4\rho^2 L_c^2 (\kappa_\gamma(\mu_e^* + \mu_m^*) + \gamma_1^*(\kappa_e + \kappa_m)) \\ 4\rho^2 L_c^4 (\kappa_\gamma(\bar{\kappa}_\gamma(\mu_e^* + \mu_m^*) + \bar{\gamma}_1^* \mu_e^* + \bar{\gamma}_1^* \mu_m^* + \kappa_e \gamma_1^* + \gamma_1^* \mu_e^*) + \gamma_1^*(\kappa_e + \kappa_m)(\bar{\gamma}_1^* + \bar{\kappa}_\gamma)) \\ 4\rho^3 L_c^4 \kappa_\gamma \gamma_1^* \\ 4\rho^3 L_c^6 \kappa_\gamma \gamma_1^* (\bar{\gamma}_1^* + \bar{\kappa}_\gamma) \end{array} \right) \quad (56)$$

Shear 45° :

$$\left(\begin{array}{c} 4\mu_c \mu_e \mu_m \\ 4\rho \mu_c (\mu_e + \mu_m) \\ 4\rho L_c^2 ((\bar{\gamma}_1 + \bar{\gamma}_2) \mu_c (\mu_e + \mu_m) + \gamma_1 \mu_c \mu_e + \gamma_2 (\mu_c (\mu_e + \mu_m) + \mu_e \mu_m)) \\ 4\rho^2 L_c^2 (\gamma_1 \mu_c + \gamma_2 (\mu_e + \mu_m)) \\ 4\rho^2 L_c^4 (\gamma_1 ((\bar{\gamma}_1 + \bar{\gamma}_2) \mu_c + \gamma_2 (\mu_c + \mu_e)) + \gamma_2 (\bar{\gamma}_1 + \bar{\gamma}_2) (\mu_e + \mu_m)) \\ 4\gamma_1 \gamma_2 \rho^3 L_c^4 \\ 4\gamma_1 \gamma_2 \rho^3 (\bar{\gamma}_1 + \bar{\gamma}_2) L_c^6 \end{array} \right) \quad (57)$$

Appendix 3

Coefficients for the dispersion curves with Curl P

For the relaxed micromorphic model with Curl P but without Curl \dot{P} , we arrived equation (38) at the dispersion polynomial

$$c_0 k^2 + c_1 k^4 - (c_2 + c_3 k^2 + c_4^* k^4) \omega^2 + (c_5 + c_6^* k^2 + c_7^* k^4) \omega^4 - (c_8 + c_9^* k^2) \omega^6 \quad (58)$$

The coefficients c_0, c_2, c_5, c_8, c_9 are identical to the one given in the section above without Curl P. Thus, we list $(c_1, c_3, c_4^*, c_6^*, c_7^*)^T$ using c_3^* and c_6^* to shorten some expressions.

Pressure 0° :

$$\left(\begin{array}{c} 2\alpha_1 L_c^2 (\kappa_e + \mu_e) (\kappa_m + \mu_m) \\ c_3^* + 2\rho \alpha_1 L_c^2 (\kappa_e + \mu_e + \kappa_m + \mu_m) \\ 2\rho \alpha_1 L_c^4 (\bar{\gamma}_1 (\kappa_e + \mu_e + \kappa_m + \mu_m) + \bar{\kappa}_\gamma (\kappa_e + \mu_e + \kappa_m + \mu_m) + (\kappa_\gamma + \gamma_1) (\kappa_e + \mu_e)) \\ c_6^* + 2\rho^2 \alpha_1 L_c^4 (\kappa_\gamma + \gamma_1) \\ 2\rho^2 \alpha_1 L_c^6 (\kappa_\gamma + \gamma_1) (\bar{\kappa}_\gamma + \bar{\gamma}_1) \end{array} \right) \quad (59)$$

Shear 0° :

$$\left(\begin{array}{c} 2\alpha_1 L_c^2 \mu_m^* (\mu_e^* + \mu_c) \\ c_3^* + 2\rho \alpha_1 L_c^2 (\mu_e^* + \mu_m^* + \mu_c) \\ 2\rho \alpha_1 L_c^4 (\bar{\gamma}_2 (\mu_e^* + \mu_m^* + \mu_c) + \bar{\gamma}_1^* (\mu_e^* + \mu_m^* + \mu_c) + (\gamma_1^* + \gamma_2) (\mu_e^* + \mu_c)) \\ c_6^* + 2\rho^2 \alpha_1 L_c^4 (\gamma_1^* + \gamma_2) \\ 2\rho^2 \alpha_1 L_c^6 (\gamma_1^* + \gamma_2) (\bar{\gamma}_1^* + \bar{\gamma}_2) \end{array} \right) \quad (60)$$

Pressure 45° :

$$\left(\begin{array}{c} 2\alpha_1 L_c^2 (\mu_e^* + \kappa_e) (\mu_m^* + \kappa_m) \\ c_3^* + 2\rho \alpha_1 L_c^2 (\mu_e^* + \mu_m^* + \kappa_e + \kappa_m) \\ 2\rho \alpha_1 L_c^4 (\bar{\kappa}_\gamma (\mu_e^* + \mu_m^* + \kappa_e + \kappa_m) + \bar{\gamma}_1^* (\mu_e^* + \mu_m^* + \kappa_e + \kappa_m) + (\gamma_1^* + \kappa_\gamma) (\mu_e^* + \kappa_e)) \\ c_6^* + 2\rho^2 \alpha_1 L_c^4 (\gamma_1^* + \kappa_\gamma) \\ 2\rho^2 \alpha_1 L_c^6 (\gamma_1^* + \kappa_\gamma) (\bar{\gamma}_1^* + \bar{\kappa}_\gamma) \end{array} \right) \quad (61)$$

Shear 45° :

$$\left(\begin{array}{c} 2\alpha_1 L_c^2 \mu_m (\mu_c + \mu_e) \\ c_3^* + 2\rho \alpha_1 L_c^2 (\mu_c + \mu_e + \mu_m) \\ 2\rho \alpha_1 L_c^4 (\bar{\gamma}_1 (\mu_c + \mu_e + \mu_m) + \bar{\gamma}_2 (\mu_c + \mu_e + \mu_m) + (\gamma_1 + \gamma_2) (\mu_c + \mu_e)) \\ c_6^* + 2(\gamma_1 + \gamma_2) \rho^2 \alpha_1 L_c^4 \\ 2(\gamma_1 + \gamma_2) \rho^2 (\bar{\gamma}_1 + \bar{\gamma}_2) \alpha_1 L_c^6 \end{array} \right) \quad (62)$$

Appendix 4

Coefficients for the dispersion curves with Curl \dot{P}

For the relaxed micromorphic model with curvature, we arrived equation (41) at the dispersion polynomial

$$c_0 k^2 + c_1 k^4 - (c_2 + c_3 k^2 + c_4 k^4) \omega^2 + (c_5 + c_6 k^2 + c_7 k^4) \omega^4 - (c_8 + c_9 k^2 + c_{10} k^4) \omega^6 \quad (63)$$

The coefficients $c_0, c_1, c_2, c_3, c_5, c_6, c_8$ are identical to the one given in the section above without Curl \dot{P} . Thus, we list $(c_4, c_6, c_7, c_9, c_{10})^T$ using $c_4^*, c_6^*, c_7^*, c_9^*$ as the coefficients from previous sections above to shorten the expressions.

Pressure 0° :

$$\left(\begin{array}{c} c_4^* + 2\rho\beta_1 L_c^4 (\kappa_e + \mu_e) (\kappa_m + \mu_m) \\ c_6^* + 2\rho^2\beta_1 L_c^4 (\kappa_e + \mu_e + \kappa_m + \mu_m) \\ c_7^* + 2\rho^2\beta_1 L_c^6 (\bar{\gamma}_1 (\kappa_e + \mu_e + \kappa_m + \mu_m) + \bar{\kappa}_\gamma (\kappa_e + \mu_e + \kappa_m + \mu_m) + (\kappa_\gamma + \gamma_1) (\kappa_e + \mu_e)) \\ c_9^* + 2\rho^3\beta_1 L_c^6 (\kappa_\gamma + \gamma_1) \\ 2\rho^3\beta_1 L_c^8 (\kappa_\gamma + \gamma_1) (\bar{\kappa}_\gamma + \bar{\gamma}_1) \end{array} \right) \quad (64)$$

Shear 0° :

$$\left(\begin{array}{c} c_4^* + 2\rho\beta_1 L_c^4 \mu_m^* (\mu_e^* + \mu_c) \\ c_6^* + 2\rho^2\beta_1 L_c^4 (\mu_e^* + \mu_m^* + \mu_c) \\ c_7^* + 2\rho^2\beta_1 L_c^6 (\bar{\gamma}_2 (\mu_e^* + \mu_m^* + \mu_c) + \bar{\gamma}_1^* (\mu_e^* + \mu_m^* + \mu_c) + (\gamma_1^* + \gamma_2) (\mu_e^* + \mu_c)) \\ c_9^* + 2\rho^3\beta_1 L_c^6 (\gamma_1^* + \gamma_2) \\ 2\rho^3\beta_1 L_c^8 (\gamma_1^* + \gamma_2) (\bar{\gamma}_1^* + \bar{\gamma}_2) \end{array} \right) \quad (65)$$

Pressure 45° :

$$\left(\begin{array}{c} c_4^* + 2\rho\beta_1 L_c^4 (\mu_e^* + \kappa_e) (\mu_m^* + \kappa_m) \\ c_6^* + 2\rho^2\beta_1 L_c^4 (\mu_e^* + \mu_m^* + \kappa_e + \kappa_m) \\ c_7^* + 2\rho^2\beta_1 L_c^6 (\bar{\kappa}_\gamma (\mu_e^* + \mu_m^* + \kappa_e + \kappa_m) + \bar{\gamma}_1^* (\mu_e^* + \mu_m^* + \kappa_e + \kappa_m) + (\gamma_1^* + \kappa_\gamma) (\mu_e^* + \kappa_e)) \\ c_9^* + 2\rho^3\beta_1 L_c^6 (\gamma_1^* + \kappa_\gamma) \\ 2\rho^3\beta_1 L_c^8 (\gamma_1^* + \kappa_\gamma) (\bar{\gamma}_1^* + \bar{\kappa}_\gamma) \end{array} \right) \quad (66)$$

Shear 45° :

$$\left(\begin{array}{c} c_4^* + 2\rho\beta_1 L_c^4 \mu_m (\mu_c + \mu_e) \\ c_6^* + 2\rho^2\beta_1 L_c^4 (\mu_c + \mu_e + \mu_m) \\ c_7^* + 2\rho^2\beta_1 L_c^6 (\bar{\gamma}_1 (\mu_c + \mu_e + \mu_m) + \bar{\gamma}_2 (\mu_c + \mu_e + \mu_m) + (\gamma_1 + \gamma_2) (\mu_c + \mu_e)) \\ c_9^* + 2(\gamma_1 + \gamma_2) \rho^3 \beta_1 L_c^6 \\ 2(\gamma_1 + \gamma_2) \rho^3 (\bar{\gamma}_1 + \bar{\gamma}_2) \beta_1 L_c^8 \end{array} \right) \quad (67)$$